J. Fluid Mech. (1987), *vol.* 174, *pp.* 39–68
Printed in Great Britain

The three-dimensional hydrodynamic interaction of a finite sphere with a circular orifice at low Reynolds number

By ZONG-YI YAN,† SHELDON WEINBAUM, PETER GANATOS

Department of Mechanical Engineering, The City College of The City University of New York, NY 10031, USA

AND ROBERT PFEFFER

Department of Chemical Engineering, The City College of The City University of New York, NY 10031, USA

(Received 21 March 1985 and in revised form 2 May 1986)

This paper proposes a combined multipole-series representation and integral-equation method for solving the low-Reynolds-number hydrodynamic interaction of a finite sphere at the entrance of a circular orifice. This method combines the flexibility of the intergral-equation method in treating complicated geometries and the accuracy and computational efficiency of the multipole-series-representation technique. For the axisymmetric case, the hydrodynamic force has been solved for the difficult case where the sphere intersects the plane of the orifice opening, which could not be treated by previous methods. For the three-dimensional case, the first numerical solutions have been obtained for the spatial variation of the twelve force and torque correction factors describing the translation or rotation of the sphere in a quiescent fluid at a pore entrance or the Sampson flow past a fixed sphere. Restricted by excessive computation time, accurate three-dimensional solutions are presented only for a sphere which is one-half the orifice diameter. However, based on an analysis of the behaviour of the force and torque correction factors for this case, approximate interpolation formulas utilizing the results on or near the orifice axis and in the far field are proposed for other diameter ratios, thus greatly extending the usefulness of the present solution.

1. Introduction

The motion of particles and macromolecules at the entrance to filters and membranes is a problem of long-standing interest in aerosol and filter technology, osmotic phenomena and the filtration of particulates in whole blood. Prominent examples are: the plasma screening effect of red cells entering small blood vessels or glass tubes; osmotic flow at the pore opening of semi-permeable or partially permeable membranes; the molecular sieving of macromolecules in the loading of plasmalemma vesicles; the interaction of micron-sized particles with the entrance geometry of a nucleopore filter; the entrance of highly deformable particles into pores such as in red-blood-cell deformability tests.

Because of the hydrodynamic interaction between the particle and the pore wall, the hydrodynamic resistance experienced by the particle can differ substantially

† Current address: Department of Mechanics, Peking University, Beijing, China.

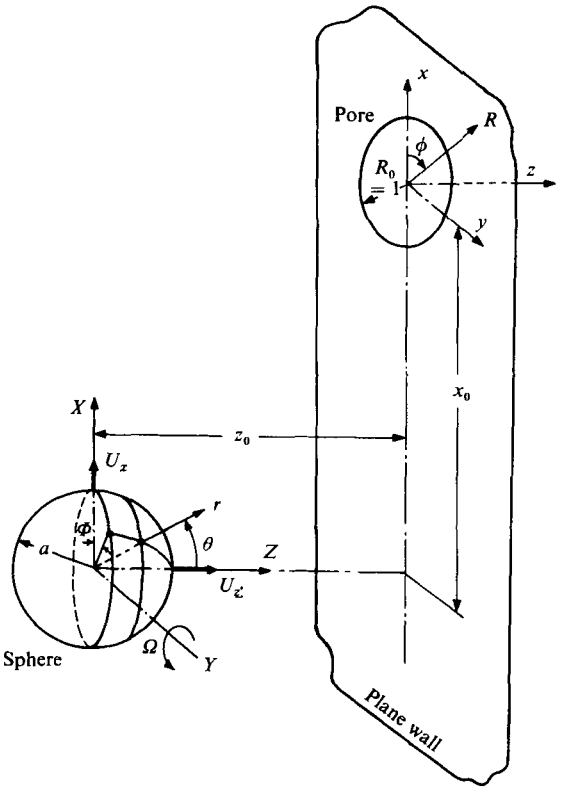

FIGURE 1. The entrance geometry.

from the Stokes resistance of a particle in an unbounded fluid. The correction factors for the hydrodynamic force and torque vary with the position and with the direction of motion. Consequently, the neutrally buoyant velocity of the particle will differ from the velocity of the fluid surrounding it and the particle diffusivity is no longer a scalar but a second-order tensor (e.g. Brenner & Gaydos 1977). The three-dimensional hydrodynamic analysis of the motion of a finite neutrally buoyant particle towards a pore is an essential input in all the problems involving entrance phenomena mentioned above.

The hydrodynamic interaction of a particle at the entrance to a finite-length pore may be approximately modelled by considering a sphere in one of the two semi-infinite half-spaces which are connected by a circular orifice in an infinitesimally thin plane wall (figure 1). As already demonstrated by the exact solution of Dagan, Weinbaum & Pfeffer (1982*a*), the flow in the exterior half-spaces is not significantly affected by the length of the pore. The Reynolds number based upon the sphere or orifice radius in these applications is very small so that the Stokes approximation of creeping flow is valid. Even with such approximations, this problem remains analytically intractable using the standard weak-interacton techniques such as the method of reflections, which has been shown to converge very slowly when the sphere-wall spacing is of the order of five sphere radii or less (Ganatos, Weinbaum & Pfeffer 1982). To attack such problems with strong hydrodynamic interactions, two numerical theories, the multipole-series-representation technique and the integral-equation method, have been developed in recent years.

The multipole-series-representation technique was first developed by Gluckman, Pfeffer & Weinbaum (1971) for unbounded axisymmetric flow and later extended to axisymmetric bounded flows (Leichtberg, Pfeffer & Weinbaum 1976; Dagan *et al.* 1982*a*) and to three-dimensional unbounded and bounded flow (Ganatos, Pfeffer & Weinbaum 1978, 1980; Ganatos *et al.* 1982). In this technique the disturbance due to a finite sphere is represented by a truncated series of internal multi-lobular disturbances and the coefficients in the series are determined by the boundary collocation method. Recently, Dagan, Weinbaum & Pfeffer (1982*b*) applied this technique to the entrance problem of the on-axis motion of a finite sphere approaching a circular orifice. They obtained accurate solutions for the hydrodynamic resistance when the sphere was located at least 1.1 times the sphere radius from the orifice plane. In their solutions different stream functions are constructed for the two half-spaces (figure 1) in terms of the unknown velocity profile at the orifice opening. The ability to analytically match the two kinematic (velocity) and dynamic (stress) fields and uniquely determine velocity profile in the plane of the orifice was crucial for their successful application of the multipole-series technique. This solution method precludes the case where the sphere partially enters the orifice. The same authors, Dagan, Weinbaum & Pfeffer (1983), also tried to extend this technique to the three-dimensional pore-entrance case. However, for this case the analytical satisfaction of dynamic continuity at the orifice proved too difficult and, therefore, they developed only an approximate model in which the rotation of the sphere and the transverse curvature effect of the orifice were neglected. Their results predicted for the first time the deviation of the trajectory of a neutrally buoyant sphere from the undisturbed fluid streamlines due to the hydrodynamic interaction with the entrance geometry of the orifice. These predictions were verified by experiment, and their theory is shown to be accurate provided that the particle centre is at least two orifice-radii away from the orifice opening.

In the integral-equation method, the velocity disturbance generated by the boundaries in the flow field is represented by the integrals of singularities distributed over the boundary surfaces (Ladyzhenskaya 1963). The application of the no-slip conditions on all surfaces, either by the collocation method (e.g. Youngren & Acrivos 1975) or by the weighted-residual technique (Lewellen 1982), leads to a set of Fredholm's integral equatons for the unknown densities of the singularity distributions. This method has been applied to Stokes flows past a particle of arbitrary shape (Youngren & Acrivos 1975), a gas bubble (Youngren & Acrivos 1976) and a deformable viscous drop (Rallison & Acrivos 1978), and to the motion of an arbitrarily positioned sphere in the flow inside a circular cylindrical pore (Lewellen 1982). This method has also been extended to creeping flows with an infinite deformable fluid–fluid interface (Lee & Leal 1982; Leal & Lee 1982). The singularities are distributed over both the finite particle surface and the infinite confining boundary, but the infinite domain of integration is truncated. This very general method so far has not been applied to problems with discontinuous boundaries such as the pore-entrance geometry.

In comparison, the multipole-series technique is very efficient and highly accurate for a finite body that conforms to some orthogonal coordinate system. However, the application of this technique to bounded flow requires the analytical satisfaction of the boundary conditions on the infinite confining boundaries, a really formidable task for many problems including the present one. In contrast, the integral-equation method is very flexible in treating boundaries of arbitrary shape including infinite boundaries. In addition, this method is especially suitable for deformable boundaries

because the local stress force on the surfaces, which is identified as the density of the Stokeslet distribution, is obtained as part of the solution. The drawbacks of this method lie in the lower accuracy and the longer computation time compared with the multipole-series technique. In this study we try to combine the two methods to make better use of each other's advantages.

As a precursor to the combined multipole-series/integral-equaton method developed herein for three-dimensional motion the authors first attempted a straightforward numerical solution of integral equation (8) (see §2.1) for the axisymmetric case where the accuracy of the results and the efficiency of the methods could be compared with the highly accurate results of Dagan *et al.* (1982*b*). This comparison, which is described in §2.2, shows that for a rigid sphere the combined method based on (9) is both more accurate and at an equivalent level of truncation requires an order of magnitude less computational time than a direct integral-equation solution. The authors have also examined the possibility of constructing a fundamental three-dimensional solution for a point force in Sampson's flow through an orifice following the related approach developed by Miyazaki & Hasimoto (1984) for a translating infinitesimal particle in a quiescent fluid. The complexity of this solution appeared to preclude its convenient use in an integral representation of the disturbance produced by a finite sphere. The present solution approach is also capable of treating the more difficult case where the sphere arbitrarily intersects the plane of the orifice opening. To our knowledge the present solutions are the first to describe this more difficult flow geometry.

Even with the efficiencies gained by the new combined approach, the three-dimensional solutions for the twelve force and torque coefficients are still very time consuming and thus accurate numerical results for all these coefficients have been obtained only for a sphere-orifice diameter ratio of one half. However, based on these accurate solutions and the asymptotic results valid on the orifice axis and in the far field, approximate interpolation formulas have been developed for the full range of particle sizes and positions. These formulas have already been used to describe the fine structure of osmosis at the entrance and exit of permeable and semi-permeable membrane pores (Yan, Weinbaum & Pfeffer 1986) and to develop a new theory for the collection efficiency of nuclepore filters which takes account of hydrodynamic and nuclepore-wall force interactions (Wang *et al.* 1986).

In §2 a combined series-integral representation of the disturbance velocity field will be derived for our entrance geometry; the axisymmetric and the three-dimensional solutions will be presented in §§3 and 4 respectively; §5 will briefly discuss the virtues and limitations of the present method.

2. Formulation

In figure 1 all the lengths are scaled relative to the orifice radius R_0. Two Cartesian coordinate systems are used: (x, y, z) is associated with the orifice and (X, Y, Z) with the sphere. For convenience, a cylindrical coordinate system (R, ϕ, z) associated with the orifice and a spherical system (r, θ, Φ) associated with the sphere are introduced.

For a creeping flow, the dimensionless Stokes equations are

$$\left.\begin{aligned} \frac{\partial^2 V_i}{\partial x_j \partial x_j} &= \frac{\partial p}{\partial x_i}, \quad (i = 1, 2, 3), \\ \frac{\partial V_k}{\partial x_k} &= 0. \end{aligned}\right\} \tag{1}$$

Here and henceforth the Einstein's convention of summation over repeated indices is adopted and (x_1, x_2, x_3) represent (x, y, z). The fluid velocity V_i is made dimensionless with respect to an arbitrary characteristic velocity U_0 and the fluid pressure p with respect to a characteristic viscous stress $\mu U_0/R_0$ where μ is the viscosity of the fluid.

Owing to the linearity of the governing equation (1), the general motion of the sphere in the symmetry plane (x, z) in zero-Reynolds-number flow can be constructed as the superposition of (i) a pure translation of the sphere with velocity $(U_x, 0, U_z)$ in a quiescent fluid; (ii) a pure rotation of the sphere with angular velocity Ω about the Y-axis in a quiescent fluid; and (iii) the flow past a stationary sphere with undisturbed velocity components V_x and V_z, which obey Sampson's solution (see (7*a–c*), at the sphere centre $(-x_0, 0, -z_0)$. The hydrodynamic force and torque on the sphere can be written as

$$\left.\begin{aligned} F_x &= 6\pi\mu a(U_x F_x^{\mathrm{t},x} + U_z F_x^{\mathrm{t},z} + a\Omega F_x^{\mathrm{r}} + V_{z0}\tilde{F}_x^{\mathrm{s}}),\\ F_z &= 6\pi\mu a(U_x F_z^{\mathrm{t},x} + U_z F_z^{\mathrm{t},z} + a\Omega F_z^{\mathrm{r}} + V_{z0}\tilde{F}_z^{\mathrm{s}}),\\ T_y &= 8\pi\mu a^2(U_x T_y^{\mathrm{t},x} + U_z T_y^{\mathrm{t},z} + a\Omega T_y^{\mathrm{r}} + V_{z0}\tilde{T}_y^{\mathrm{s}}), \end{aligned}\right\} \tag{2}$$

where V_{z0} is the flow velocity at the centre of the orifice opening and will be given by (21*b*); $F_x^{\mathrm{t},z}, F_x^{\mathrm{r}}, \ldots, \tilde{T}_y^{\mathrm{s}}$ are twelve force and torque correction factors obtained from the solutions of the three separated problems mentioned above, with the superscripts t, r, s denoting the three problems in sequence. These factors account for the hydrodynamic interactions between the sphere and the orifice entrance geometry. For a neutrally buoyant sphere carried by the flow, these equations with $F_x = F_z = T_y = 0$ yield three relations to determine U_x, U_z and Ω.

Now let us mathematically formulate the problem in order to determine the force and torque correction factors.

2.1. *Integral representation*

Ladyzhenskaya (1963) derived a Green's formula for Stokes flow as follows:

$$\iiint_\Omega \left\{ V_i(\boldsymbol{y}) \left[\frac{\partial^2 u_i^k(\boldsymbol{x},\boldsymbol{y})}{\partial y_j \partial y_j} - \frac{\partial p^k(\boldsymbol{y},\boldsymbol{x})}{\partial y_i} \right] - u_i^k(\boldsymbol{x},\boldsymbol{y}) \left[\frac{\partial^2 V_i(\boldsymbol{y})}{\partial y_j \partial y_j} - \frac{\partial p(\boldsymbol{y})}{\partial y_i} \right] \right\} \mathrm{d}\Omega_y$$

$$= \iint_{\partial\Omega} \{ V_i(\boldsymbol{y})\, T_{ij}[\boldsymbol{u}^k(\boldsymbol{x},\boldsymbol{y})]\, n_j(\boldsymbol{y}) - u_i^k(\boldsymbol{x},\boldsymbol{y})\, T_{ij}[\boldsymbol{V}(\boldsymbol{y})]\, n_j(\boldsymbol{y}) \}\, \mathrm{d}S_y, \tag{3}$$

Here $V_i(\boldsymbol{x})$ and $p(\boldsymbol{x})$ are the actual solutions to (1) for a field point $\boldsymbol{x}$ and $u_i^k(\boldsymbol{x},\boldsymbol{y})$ and $p^k(\boldsymbol{x},\boldsymbol{y})$ are the solutions at the field point $\boldsymbol{x}$ due to a fictitious Stokeslet (point force) in the kth direction at point $\boldsymbol{y}$. These solutions are given by

$$u_i^k(\boldsymbol{x},\boldsymbol{y}) = -\frac{1}{8\pi}\left[\frac{\delta_{ik}}{r_{xy}} + \frac{(x_i - y_i)(x_k - y_k)}{r_{xy}^3} \right], \tag{4a}$$

$$p^k(\boldsymbol{x},\boldsymbol{y}) = \frac{y_k - x_k}{4\pi r_{xy}^3}, \tag{4b}$$

where $r_{xy} = |\boldsymbol{x} - \boldsymbol{y}|$ and δ_{ik} is the Kronecker delta. $T_{ij}[\boldsymbol{v}(\boldsymbol{y})]$ and $T_{ij}[\boldsymbol{u}^k(\boldsymbol{x},\boldsymbol{y})]$ represent the stress tensors associated with $\boldsymbol{V}(\boldsymbol{y})$ and $\boldsymbol{u}^k(\boldsymbol{y})$ respectively:

$$T_{ij}[\boldsymbol{V}(\boldsymbol{y})] = -\delta_{ij}\, p(\boldsymbol{y}) + \frac{\partial V_i(\boldsymbol{y})}{\partial y_j} + \frac{\partial V_j(\boldsymbol{y})}{\partial y_i}, \tag{4c}$$

$$T_{ij}[\boldsymbol{u}^k(\boldsymbol{x},\boldsymbol{y})] = -\delta_{ij}\, p^k(\boldsymbol{y},\boldsymbol{x}) + \frac{\partial u_i^k(\boldsymbol{x},\boldsymbol{y})}{\partial y_j} + \frac{\partial u_j^k(\boldsymbol{x},\boldsymbol{y})}{\partial y_i}, \tag{4d}$$

and n_j is the exterior normal vector (with respect to the flow field Ω) to the boundary $\partial\Omega$ and therefore points *inward* from the body surface. The subscript y in $\mathrm{d}S_y$ and $\mathrm{d}\Omega_y$ indicates that the integrations are to be performed over $\boldsymbol{y}$. With the help of the Green's formula the flow velocity $\boldsymbol{V}(\boldsymbol{x})$ can be expressed in terms of the so-called single- and double-layer potentials $V_i^{(1)}(\boldsymbol{x})$ and $V_i^{(2)}(\boldsymbol{x})$:

$$V_i(\boldsymbol{x}) = V_i^{(1)}(\boldsymbol{x}) + V_i^{(2)}(\boldsymbol{x}), \tag{5a}$$

$$\left.\begin{aligned} V_i^{(1)}(\boldsymbol{x}) &= -\iint_{\partial\Omega} u_i^k(\boldsymbol{x},\boldsymbol{y})\, T_{kj}[\boldsymbol{V}(\boldsymbol{y})]\, n_j(\boldsymbol{y})\, \mathrm{d}S_y, \\ &= -\iint_{\partial\Omega} u_i^k(\boldsymbol{x},\boldsymbol{y}) f_k(\boldsymbol{y})\, \mathrm{d}S_y, \\ &= \frac{1}{8\pi}\iint_{\partial\Omega}\left[\frac{\delta_{ik}}{r_{xy}} + \frac{(x_i-y_i)(x_k-y_k)}{r_{xy}^3}\right] f_k(\boldsymbol{y})\, \mathrm{d}S_y, \end{aligned}\right\} \tag{5b}$$

$$\left.\begin{aligned} V_i^{(2)}(\boldsymbol{x}) &= \iint_{\partial\Omega} T_{ij}[\boldsymbol{u}^k(\boldsymbol{x},\boldsymbol{y})]\, V_k(\boldsymbol{y})\, n_j(\boldsymbol{y})\, \mathrm{d}S_y, \\ &= -\frac{3}{4\pi}\iint_{\partial\Omega} \frac{(x_i-y_i)(x_j-y_j)(x_k-y_k)}{r_{xy}^5}\, V_k(\boldsymbol{y})\, n_j(\boldsymbol{y})\, \mathrm{d}S_y, \end{aligned}\right\} \tag{5c}$$

where
$$f_k(\boldsymbol{y}) = T_{kj}[\boldsymbol{V}(\boldsymbol{y})]\, n_j(\boldsymbol{y}) \tag{5d}$$

represents the actual local stress force in the k-direction. It has been shown that, if $\partial\Omega$ is a Lyapunov surface, the single-layer potential $V_i^{(1)}(\boldsymbol{x})$ is continuous in Ω and $\partial\Omega$ but the double-layer potential $V_i^{(2)}(\boldsymbol{x})$ undergoes a discontinuity across $\partial\Omega$:

$$\lim_{\boldsymbol{x}\to\boldsymbol{x}_0} V_i^{(2)}(\boldsymbol{x}) = V_i^{(2)}(\boldsymbol{x}_0) + \tfrac{1}{2}V_i(\boldsymbol{x}_0). \quad \text{when } \boldsymbol{x}\in\Omega, \quad \boldsymbol{x}_0\in\partial\Omega. \tag{5d}$$

The factor $\frac{1}{2}$ applies only for smooth surfaces.

It is noted that (3) is derived under the assumption that both $\boldsymbol{V}(\boldsymbol{x})$ and $p(\boldsymbol{x})$ should vanish at infinity. Therefore it cannot be applied directly to our flow in figure 1, where p_∞ and $p_{-\infty}$ may be different. This difficulty is easily eliminated by decomposing the present problem into the sum of Sampson's solution for a flow through a circular orifice (with superscript S) and a remaining disturbance (primed quantities), where both $\boldsymbol{V}'(\boldsymbol{x})$ and $p'(\boldsymbol{x})$ vanish at infinity, namely

$$\left.\begin{aligned} V_i(\boldsymbol{x}) &= V_i^{\mathrm{S}}(\boldsymbol{x}) + V_i'(\boldsymbol{x}), \\ p(\boldsymbol{x}) &= p^{\mathrm{S}}(\boldsymbol{x}) + p'(\boldsymbol{x}). \end{aligned}\right\} \tag{6}$$

The Sampson solution is given as (Happel & Brenner 1973, p. 153)

$$V_R^{\mathrm{S}}(\boldsymbol{x}) = -\frac{3q}{8\pi} z\frac{\zeta}{R}(R_1-R_2)\left(\frac{1}{R_1}-\frac{1}{R_2}\right), \tag{7a}$$

$$V_z^{\mathrm{S}}(\boldsymbol{x}) = \frac{3q\zeta}{8\pi R}(R_1-R_2)\left(\frac{R-1}{R_1}-\frac{R+1}{R_2}\right), \tag{7b}$$

$$p^{\mathrm{S}}(\boldsymbol{x}) = \frac{3q}{\pi}\left(\frac{\lambda}{\lambda^2+\zeta^2}+\tan^{-1}\lambda\right). \tag{7c}$$

Here the dimensionless volume flux q is related to the pressure difference $(p_{-\infty}-p_\infty)$

and the oblate spheroidal coordinates (λ, ζ) are related to the cylindrical coordinates (R, ϕ, z), as follows:

$$q = \tfrac{1}{3}(p_{-\infty} - p_{\infty}), \tag{7d}$$

$$\lambda = [\tfrac{1}{4}(R_1 + R_2)^2 - 1], \tag{7e}$$

$$\zeta = [1 - \tfrac{1}{4}(R_2 - R_1)^2], \tag{7f}$$

$$R_1 = [z^2 + (R-1)^2]^{\frac{1}{2}}, \tag{7g}$$

$$R_2 = [z^2 + (R+1)^2]^{\frac{1}{2}}. \tag{7h}$$

Now the Green's formula (3) can be applied to the disturbance field $\boldsymbol{V}'(\boldsymbol{x})$ and $p'(\boldsymbol{x})$. The plane wall of the orifice as shown in figure 1 has no definite tangent plane at the edge of the orifice and, therefore, is not a Lyapunov surface as required in deriving equation (3). However, the flow field in figure 1 can be divided by the orifice opening and wall into two semi-infinite regions and then the boundary of each region consists of Lyapunov surfaces. Applying the Green's formula (3) to each region and then adding the resulting integral expressions, we obtain

$$V_i'(\boldsymbol{x}) = -\iint_{S_p} u_i^k(\boldsymbol{x}, \boldsymbol{y})\, T_{kj}^{(p)}[\boldsymbol{V}'(\boldsymbol{y})]\, n_j^{(p)}(\boldsymbol{y})\, \mathrm{d}S_y + \iint_{S_p} T_{ij}[\boldsymbol{u}^k(x, y)] \times V_k'^{(p)}(\boldsymbol{y})\, n_j^{(p)}(\boldsymbol{y})\, \mathrm{d}S_y - \iint_{S_w-} U_i^k(\boldsymbol{x}, \boldsymbol{y}) f_k^{(w)}(\boldsymbol{y})\, \mathrm{d}S_y, \tag{8a}$$

where S_p denotes the sphere surface, and the density function $f_k^{(w)}(\boldsymbol{y})$ in the single-layer potential on the plane wall S_w- represents the stress difference across the wall:

$$f_k^{(w)}(\boldsymbol{y}) = T_{kz}^{(-)}[\boldsymbol{V}'(\boldsymbol{y})] - T_{kz}^{(+)}[\boldsymbol{V}'(\boldsymbol{y})], \quad k = 1, 2, 3. \tag{8b}$$

Note that no double-layer potential on the plane wall S_w- appears in equation (8*a*) because the $\boldsymbol{V}'(\boldsymbol{y})$ is identically zero on S_w-. The second integral in (8*a*), although known, can be converted into a single-layer potential and combined with the first integral following the procedure in Rallison & Acrivos (1978). One defines a fictitious fluid motion inside the sphere with velocity $\boldsymbol{V}'(\boldsymbol{y})$ on S_p, relates the single- and double-layer potentials for this problem, absorbs the former into the first integral in (8*a*) and redefines the unknown stress distribution. Since an alternative expression for the first two integrals in (8*a*) will be used, we shall not pursue this simplification further.

Equation (8*a*) is a unified expression, valid for any point $\boldsymbol{x}$ in the flow field. There is furthermore no restriction on the position of the sphere centre. This will enable us to find the solution even if the sphere intersects the orifice opening, while such cases could not be treated by any previous method.

2.2. *The combined multipole-series/integral representation*

While the integral equation (8*a*) could be solved numerically to determine the unknown stress functions $T_{kj}^{(p)}(\boldsymbol{V}'(\boldsymbol{y}))$ and $f_k^{(w)}(\boldsymbol{y})$ by satisfying the no-slip boundary conditions on S_p and S_w-, the approximations used to represent these functions usually produce considerable inaccuracy in calculating the force and torque, which are our primary goals. On the other hand, in a variety of applications using the multipole-series truncation technique, Lamb's spherical harmonic-series solution provided high accuracy in evaluating the force and torque coefficients using relatively

few terms in the series truncation (Weinbaum 1981). The multipole-series representation provides the important additional advantage that each force and torque coefficient can be expressed in terms of a single unknown constant coefficient in the series (see (10a, b) below). In contrast, for the orifice wall there is no convenient set of fundamental eigenfunctions which can be used to analytically satisfy the boundary conditions on the surface of the orifice for three-dimensional motion as was done in Dagan *et al.* (1982b) for axisymmetric flow.

To test these ideas preliminary calculations were first performed for the simpler axisymmetric problem where the results could be compared with the accurate series solutions in Dagan *et al.* (1982b) where the boundary conditions on the orifice wall are satisfied exactly. Two solution approaches were tried, one where the integral equation (8) was solved numericallly and one where a series of cylindrically symmetric eigenfunctions derived from (9a) below was used to represent the disturbance produced by the sphere. The second solution procedure is described in detail in §2.3. The integral describing the disturbance produced by the wall was treated the same in both cases. The solutions using both methods are compared in table 1 with the results in Dagan *et al.* (1982b) both for a sphere moving in a quiescent fluid and for Sampson's flow past a stationary sphere. M_1 refers to the number of equal segments of generating arc into which the sphere was divided when integral equation (8a) was solved or the number of terms retained in the series representation when (9a) was used. N_2 is the number of radial divisions used for the orifice wall. It is clear from the results in table 1 that better accuracy could be obtained using a significantly smaller value of M_1 when the sphere was represented by the multipole series. Furthermore, the computation time using (8a) was 5 to 10 times longer than the computation time using (9a). For the much more complicated three-dimensional case we have every reason to expect that the method using (9a) will be far superior to that using (8a).†

In view of the above arguments, we shall represent the disturbance on the sphere surface by Lamb's series solution, instead of the first two integrals (the hydrodynamic potentials on S_p) in (8a), while retaining the third integral (the single-layer potential on S_w-) in (8a) to represent the disturbance on the orifice wall. This would enable us to evaluate the force and torque on the sphere with higher accuracy while avoiding the difficulty of analytically satisfying the boundary conditions on the orifice wall. We thus replce (8a) by

$$V_i'(\boldsymbol{x}) = \sum_{n=1}^{\infty}\sum_{m=0}^{n}\left[B_{mn}\,B_{mn}^{(i)}(r,\theta,\Phi)+C_{mn}\,C_{mn}^{(i)}(r,\theta,\Phi)+E_{mn}\,E_{mn}^{(i)}(r,\theta,\Phi)\right]$$
$$+\frac{1}{8\pi}\iint_{S_w-}\left[\frac{\delta_{ik}}{r_{xy}}+\frac{(x_i-y_i)\,(x_k-y_k)}{r_{xy}^3}\right]f_k^{(w)}(\boldsymbol{y})\,\mathrm{d}S_y, \quad (i=1,2,3), \quad (9a)$$

where

$$B_{mn}^{(1)}(r,\theta,\Phi)=\frac{1}{r^{n+1}}\left[-\sin\theta\sin\Phi\,\frac{\mathrm{d}P_n^m(\xi)}{\mathrm{d}\xi}\sin m\Phi+m\,\frac{\cos\Phi}{\tan\theta}\,P_n^m(\xi)\cos m\Phi\right], \quad (9b)$$

† This conclusion is only valid for rigid spheres where there is no discontinuity in velocity boundary conditions on the sphere surface. For the axisymmeteric low-Re motion of a bubble with a stagnant cap of surfactants in an unbounded fluid it is evident from the comparison of the exact solution of Sadhal & Johnson (1983), with the truncated spherical harmonic series of Davis & Acrivos (1966) that the spherical harmonic series is not an efficient representation for this case. The first author has recently completed in conjuction with Z. Dagan and H. Shan a study of the axisymmetric motion of a gas bubble or a bubble with a stagnant surfactant cap towards an orifice. In this study it was more efficient to solve the integral equation (8a) numerically rather than (9a).

F_z^t for a moving sphere in quiescent fluid

	$a/R_0 = 0.1$			$a/R_0 = 1.0$			$a/R_0 = 10.0$		
z_0/a	(8*a*)†	(9*a*)‡	Dagan‖	(8*a*)	(9*a*)	Dagan	(8*a*)	(9*a*)	Dagan
10.0	−1.086	−1.072	−1.060	−1.125	−1.126	−1.126	−1.126	−1.125	−1.125
5.0	−1.084	−1.067	−1.053	−1.280	−1.281	−1.280	−1.284	−1.284	−1.285
2.0	−1.061	−1.054	−1.051	−1.871	−1.865	−1.806	−2.123	−2.125	−2.125

F_z^s for Sampson's flow past a stationary sphere

10.0	0.5470	0.5344	0.5280	0.01108	0.01110	0.01109	0.000113	0.000112	0.000112
5.0	0.8800	0.8485	0.8380	0.05046	0.04918	0.04860	0.000529	0.000513	0.000508
2.0	1.0420	1.0069	1.0036	0.4446	0.3593	0.3275	0.00666	0.00565	0.00566

TABLE 1. Comparison of the axisymmetric results for a solid sphere

† Using equation (8*a*), with $M_1 = 25$, $N_2 = 20$; Yan, Shan & Dagan (1987).
‡ Using equation (9*a*), with $M_1 = 4$–10, $N_2 = 14$–20 (the present paper).
‖ Dagan *et al.* (1982*b*).

$$C_{mn}^{(1)}(r,\theta,\Phi) = \frac{1}{r^{n+2}}\left[-\left((n+1)P_n^m(\xi)+\xi\frac{\mathrm{d}P_n^m(\xi)}{\mathrm{d}\xi}\right)\sin\theta\cos\Phi\cos m\Phi + m\frac{\sin\Phi}{\sin\theta}P_n^m(\xi)\sin m\Phi\right], \quad (9c)$$

$$E_{mn}^{(1)}(r,\theta,\Phi) = \frac{1}{2(2n-1)r^n}\left[\left((n+1)P_n^m(\xi)+\frac{n-2}{n}\xi\frac{\mathrm{d}P_n^m(\xi)}{\mathrm{d}\xi}\right)\sin\theta\cos\Phi\cos m\Phi - \frac{m(n-2)}{n}\frac{\sin\Phi}{\sin\theta}P_n^m(\xi)\sin m\Phi\right], \quad (9d)$$

$$B_{mn}^{(2)}(r,\theta,\Phi) = \frac{1}{r^{n+1}}\left[\sin\theta\cos\Phi\frac{\mathrm{d}P_n^m(\xi)}{\mathrm{d}\xi}\sin m\Phi + m\frac{\sin\Phi}{\sin\theta}P_n^m(\xi)\cos m\Phi\right], \quad (9e)$$

$$C_{mn}^{(2)}(r,\theta,\Phi) = \frac{1}{r^{n+2}}\left[-\left((n+1)P_n^m(\xi)+\xi\frac{\mathrm{d}P_n^m(\xi)}{\mathrm{d}\xi}\right)\sin\theta\sin\Phi\cos m\Phi - m\frac{\cos\Phi}{\sin\theta}P_n^m(\xi)\sin m\Phi\right], \quad (9f)$$

$$E_{mn}^{(2)}(r,\theta,\Phi) = \frac{1}{2(2n-1)r^n}\left[\left((n+1)P_n^m(\xi)+\frac{n-2}{n}\xi\frac{\mathrm{d}P_n^m(\xi)}{\mathrm{d}\xi}\right)\sin\theta\sin\Phi\cos m\Phi + \frac{m(n-2)}{n}\frac{\cos\Phi}{\sin\theta}P_n^m(\xi)\sin m\Phi\right], \quad (9g)$$

$$B_{mn}^{(3)}(r,\theta,\Phi) = -\frac{m}{r^{n+1}}P_n^m(\xi)\cos m\Phi, \quad (9h)$$

$$C_{mn}^{(3)}(r,\theta,\Phi) = \frac{1}{r^{n+2}}(m-n-1)P_{n+1}^m(\xi)\cos m\Phi, \quad (9i)$$

$$E_{mn}^{(3)}(r,\theta,\Phi) = \frac{1}{2n(2n-1)r^n}[2(n+1)\xi P_n^m(\xi)+(m-2)(n-m+1)P_{n+1}^m(\xi)]\cos m\Phi, \quad (9j)$$

$$\xi = \cos\theta, \quad (9k)$$

$$\frac{\mathrm{d}P_n^m(\xi)}{\mathrm{d}\xi} = \frac{1}{1-\xi^2}\left[(m+1)\,\xi P_n^m(\xi) - (n-m+1)\,P_{n+1}^m(\xi)\right]. \tag{9l}$$

Here $P_n^m(\xi)$ is the associated Legendre polynomial. The introduction of the Lamb's series reduces the amount of numerical integration considerably. The evaluation of the force and torque on the sphere is also simplified since these can be related to the lowest-order coefficients in the spherical harmonic series:

$$\boldsymbol{F} = -4\pi(E_{11}\,\boldsymbol{i} + E_{01}\,\boldsymbol{k}), \tag{10a}$$

$$\boldsymbol{T} = -8\pi B_{11}\,\boldsymbol{j}. \tag{10b}$$

The no-slip conditions on the sphere surface and orifice wall are

$$V_i'(r=a) = V_i'^{(\mathrm{p})}(\theta, \Phi), \quad (\text{on } S_\mathrm{p}); \tag{11a}$$

$$V_i'(R \geqslant 1, \quad z=0) = 0, \quad (\text{on } S_\mathrm{w}-); \tag{11b}$$

where

$$V_x'^{(\mathrm{p})}(\theta, \Phi) = U_x + a\Omega\cos\theta - V_R^\mathrm{S}(a, \theta, \Phi), \tag{11c}$$

$$V_z'^{(\mathrm{p})}(\theta, \Phi) = U_z - a\Omega\sin\theta\cos\Phi - V_z^\mathrm{S}(a, \theta, \Phi). \tag{11d}$$

$V_R^\mathrm{S}(\boldsymbol{x})$ and $V_z^\mathrm{S}(\boldsymbol{x})$ are evaluated by $(7a, b)$; U_x, U_z and Ω are the translational and angular velocities of the sphere. In the next two subsections we shall discuss how to apply these boundary conditions for the axisymmetric and three-dimensional cases, respectively, to determine the unknown function $f_k^{(\mathrm{w})}(\boldsymbol{y})$ and the unknown coefficients B_{mn}, C_{mn} and E_{mn} in $(9a)$.

2.3. *The collocation technique*

For the axisymmetric case we apply the no-slip conditions at M_1 discrete points on the sphere surface S_p and at N_2 points on the plane wall $S_\mathrm{w}-$. All the points are located in the same meridian plane, for convenience take $\phi = \Phi = 0$. Owing to the axial symmetry, the unknown $f_k^{(\mathrm{w})}(\boldsymbol{y})$ is of the following form:

$$\left.\begin{aligned} f_1^{(\mathrm{w})}(\boldsymbol{y}) &= f_R(\tilde{R})\cos\tilde{\phi}, \\ f_2^{(\mathrm{w})}(\boldsymbol{y}) &= f_R(\tilde{R})\sin\tilde{\phi}, \\ f_3^{(\mathrm{w})}(\boldsymbol{y}) &= f_z(\tilde{R}), \end{aligned}\right\} \tag{12}$$

where $f_R(\tilde{R})$ and $f_z(\tilde{R})$ are unknown functions of $\tilde{R}$ and $\boldsymbol{y} = (\tilde{R}, \tilde{\phi}, 0)$ is the location of the Stokeslet on $S_\mathrm{w}-$. In $(9a)$, only the terms with $m = 0$ in the series are retained for the axisymmetric case. Note that $B_{mn}^{(i)}(r, \theta, \Phi) \equiv 0$ when $m = 0$. The integral equations that result after the no-slip conditions are applied cannot be solved analytically for $f_R(\tilde{R})$, $f_z(\tilde{R})$, C_{0n} and E_{0n}. To reduce the integral equations to a set of linear algebraic equations, which can be solved numerically, we first truncate the infinite domain of integration $1 \leqslant \tilde{R} < \infty$ on $S_\mathrm{w}-$ into a large finite region $1 \leqslant \tilde{R} \leqslant R_\mathrm{u}$ and then divide this region into (N_2-2) *intervals* $(\hat{R}_{n-1}, \hat{R}_n)$, assuming that

$$\hat{R}_1 = 1.0; \quad \hat{R}_n = \tfrac{1}{2}(R_n + R_{n+1}) \quad \text{for } n = 2, 3, \ldots, N_2-2; \quad \hat{R}_{N_2-1} = R_\mathrm{u}; \tag{13}$$

where $1 \leqslant R_1 < R_2 < \ldots < R_{N_2} \leqslant R_\mathrm{u}$ are radial coordinates of the chosen collocation points on the orifice plane. For each of the intervals, the unknown $f_R(\tilde{R})$ and $f_z(\tilde{R})$ are approximated by the piecewise quadratic interpolation:

$$f_k(\tilde{R}) = \sum_{\alpha=1}^{3} f_k(R_{n-2+\alpha})\,(A_\alpha^{(n)}\,\tilde{R}^2 + B_\alpha^{(n)}\,\tilde{R} + C_\alpha^{(n)}),$$

when

$$\hat{R}_{n-1} \leqslant \tilde{R} < \hat{R}_n, \quad (n = 2, 3, \ldots, N_2-1). \tag{14}$$

Here $f_k(\tilde{R})$ can be either $f_R(\tilde{R})$ or $f_z(\tilde{R})$ and the coefficients $A_\alpha^{(n)}, B_\alpha^{(n)}, C_\alpha^{(n)}$ can be determined from the condition that $f_k(\tilde{R}) = f_k(R_n)$ at $\tilde{R} = R_n$. With (14) substituted into the integral equation and the series in (9*a*) truncated to $n \leqslant M_1$, the no-slip conditions, when applied at the designated collocation points on S_p and S_w-, yield the following linear system of equations ($i = 1$ and 3 only):

$$\sum_{n=1}^{M_1} [C_{0n} C_{0n}^{(i)}(a, \theta_p, 0) + E_{0n} E_{0n}^{(i)}(a, \theta_p, 0)]$$

$$+ \frac{1}{8\pi} \sum_{n=2}^{N_2-1} \sum_{\alpha=1}^{3} [f_R(R_{n-2+\alpha}) G_{iR}^{n\alpha}(R_p, 0, z_p) + f_z(R_{n-2+\alpha}) G_{iz}^{n\alpha}(R_p, 0, z_p)]$$

$$= V_i'^{(p)}(\theta_p, 0), \quad \text{at } \boldsymbol{x} = (a, \theta_p, 0) = (R_p, 0, z_p) \in S_p, \quad p = 1, 2, \ldots, M_1; \quad (15a)$$

$$\sum_{n=1}^{M_1} [C_{0n} C_{0n}^{(i)}(r_q, \theta_q, 0) + E_{0n} E_{0n}^{(i)}(r_q, \theta_q, 0)]$$

$$+ \frac{1}{8\pi} \sum_{n=2}^{N_2-1} \sum_{\alpha=1}^{3} [f_R(R_{n-2+\alpha}) G_{iR}^{n\alpha}(R_q, 0, 0) + f_z(R_{n-2+\alpha}) G_{iz}^{n\alpha}(R_q, 0, 0)]$$

$$= 0, \quad \text{at } \boldsymbol{x} = (r_q, \theta_q, 0) = (R_q, 0, 0) \in S_w-, \quad q = 1, 2, \ldots, N_2; \quad (15b)$$

where $V_i'^{(p)}(\theta, \Phi)$ are given by (11*a*, *b*); $C_{0n}^{(i)}(r, \theta, \Phi)$ and $E_{0n}^{(i)}(r, \theta, \Phi)$ by (9*c*, *d*, *i*, *j*) and

$$G_{iR}^{n\alpha}(R, \phi, z) = A_\alpha^{(n)} \sum_{j=1}^{2} H_{ij}^{(3)}(R, \phi, z; \hat{R}_{n-1}, \hat{R}_n; 1) + B_\alpha^{(n)} \sum_{j=1}^{2} H_{ij}^{(2)}(R, \phi, z; \hat{R}_{n-1}, \hat{R}_n; 1)$$

$$+ C_\alpha^{(n)} \sum_{j=1}^{2} H_{ij}^{(1)}(R, \phi, z; \hat{R}_{n-1}, \hat{R}_n; 1); \quad (16a)$$

$$G_{iz}^{n\alpha}(R, \phi, z) = A_\alpha^{(n)} H_{i3}^{(3)}(R, \phi, z; \hat{R}_{n-1}, \hat{R}_n; 0) + B_\alpha^{(n)} H_{i3}^{(2)}(R, \phi, z; \hat{R}_{n-1}, \hat{R}_n; 0)$$

$$+ C_\alpha^{(n)} H_{i3}^{(1)}(R, \phi, z; \hat{R}_{n-1}, \hat{R}_n; 0); \quad (16b)$$

$$H_{ij}^{(\beta)}(R, \phi, z; b_1, b_2; m)$$

$$= \begin{cases} \displaystyle\int_{b_1}^{b_2} \int_0^{2\pi} \left[\frac{\delta_{ij}}{r_{xy}} + \frac{(x_i - y_i)(x_j - y_j)}{r_{xy}^3} \right] \cos m\phi \, \tilde{R}^\beta \, \mathrm{d}\tilde{\phi} \, \mathrm{d}\tilde{R}, & \text{when } j = 1 \text{ or } 3; \\ \displaystyle\int_{b_1}^{b_2} \int_0^{2\pi} \left[\frac{\delta_{ij}}{r_{xy}} + \frac{(x_i - y_i)(x_j - y_j)}{r_{xy}^3} \right] \sin m\phi \, \tilde{R}^\beta \, \mathrm{d}\tilde{\phi} \, \mathrm{d}\tilde{R}, & \text{when } j = 2. \end{cases} \quad (16c)$$

Equations (15*a*, *b*) constitute $2(M_1 + N_2)$ equations, which can be solved for the $2(M_1 + N_2)$ unknowns: C_{0n}, E_{0n} ($n = 1, 2, \ldots, M_1$) and $f_R(R_n), f_z(R_n)$ ($n = 1, 2, \ldots, N_2$). The force and torque on the sphere are then found from (10*a*, *b*).

The most tedious and time-consuming part of this work is the evaluation of integrals $H_{ij}^{(\beta)}(R, \phi, z; b_1, b_2; m)$ as defined by (16*c*). For example, if we take $M_1 = 10$ and $N_2 = 20$, then we have to evaluate $18(M_1 + N_2)(N_2 - 2) = 9720$ such integrals. Fortunately, the integration over $\tilde{\phi}$ can be performed analytically and the results expressed in terms of complete elliptic integrals. For the collocation points on S_w- (where $z = 0$), we are also able to perform the integration over $\tilde{R}$ analytically by expanding the elliptic integrals into various power series of their modli or complementary moduli. For the collocation points on S_p, part of the integration over $\tilde{R}$ has

to be carried out numerically. In either case $H_{ij}^{(\beta)}(R,\phi,z;b_1,b_2;m)$ can be expressed in the following forms:

$$H_{ij}^{(\beta)}(R,\phi,z;b_1,b_2;m)=\begin{cases} g_{ij}^a(R;b_1,b_2;m,\beta)\cos m\phi+g_{ij}^b(R;b_1,b_2;m,\beta)\cos(m-k)\phi \\ \qquad +g_{ij}^c(R;b_1,b_2;m,\beta)\cos(m+k)\phi, \quad \text{when } i=1 \text{ or } 3; \\ g_{ij}^a(R;b_1,b_2;m,\beta)\sin m\phi+g_{ij}^b(R;b_1,b_2;m,\beta)\sin(m-k)\phi \\ \qquad +g_{ij}^c(R;b_1,b_2;m,\beta)\sin(m+k)\phi, \quad \text{when } i=2. \end{cases} \tag{17}$$

Here $k=1$ for $i=3$ or $j=3$ and $k=2$ otherwise. The derivation of these formulas is both lengthy and non-trivial. A brief description will be given in the Appendix.

2.4. *The mixed weighted-residual and collocation technique*

For the three-dimensional case, we expand $f_k^{(w)}(y)$ in the form of Fourier series:

$$f_k^{(w)}(y)=\begin{cases} \sum_{m=0}^{\infty} f_{km}(\tilde{R})\cos m\tilde{\phi}, & \text{when } k=1 \text{ or } 3; \\ \sum_{m=1}^{\infty} f_{km}(\tilde{R})\sin m\tilde{\phi}, & \text{when } k=2. \end{cases} \tag{18}$$

The collocation technique described in last subsection can also be used for this case, in principle. However, the chosen collocation points have to be located in more than just the meridian plane. The previous work (Ganatos *et al.* 1978) and our numerical tests show that the results for the force and torque on the sphere are sensitive to the configuration of the collocation pints. It is impractical to place a sufficient number of collocation points so that the distribution of the points is reasonably dense on the infinite plane wall S_w- (even if it is truncated). Therefore, we shall use a weighted-residual technique for the plane wall S_w-, but retain the collocation technique on the sphere surface S_p. The collocation technique presents little difficulty on S_p, whereas the weighted-residual technique would require a much greater amount of numerical integration on S_p.

The weighted-residual technique is based on the idea that the no-slip conditions should be satisfied not at discrete boundary points, but rather on the continuous boundary in the sense of weighted averaging. In our present problem the no-slip conditions (11*b*) on S_w- can be written as follows:

$$V_i'(r,\phi,0)=0, \quad \text{when } R\geqslant 1, \quad 0\leqslant\phi<2\pi. \tag{19a}$$

Choose a family of weight functions $w_{il}(\phi)$, $l=0,1,2,\ldots$. Now multiplying (19*a*) by one of the $w_{il}(\phi)$ and integrating it over ϕ from 0 to 2π, we have

$$\int_0^{2\pi} V_i'(R,\phi,0)\,w_{il}(\phi)\,\mathrm{d}\phi=0, \quad \text{when } R\geqslant 1. \tag{19b}$$

In principle, we may also perform a similar weighted averaging in the R-direction. However, we shall not do this here because it would require an excessive amount of numerical integration. Instead, we choose a number of values R_n, as we did for the axisymmetric case, and require that (19*b*) should be satisfied for these discrete R_n, i.e.

$$\int_0^{2\pi} V_i'(R_n,\phi,0)\,w_{il}(\phi)\,\mathrm{d}\phi=0, \quad n=1,2,3,\ldots,N_2. \tag{19c}$$

Thus the no-slip conditions are satisfied at discrete rings on S_w-, in some average sense. In this work we choose

$$w_{il}(\phi) = \begin{cases} \cos l\phi, & \text{when } i = 1 \text{ or } 3; \\ \sin l\phi, & \text{when } i = 2. \end{cases} \tag{19d}$$

One advantage of such a choice is to make use of the orthogonality of trigonometric functions in evaluating the integrals in ϕ of terms like $H_{ij}^{(\beta)}(R, \phi, z; b_1, b_2; m)$ as given by (17), thus avoiding a lot of numerical integration. However, the $B_{mn}^{(i)}(r, \theta, \Phi)$, $C_{mn}^{(i)}(r, \theta, \Phi)$ and $E_{mn}^{(i)}(r, \theta, \Phi)$ terms in the expression (9a) for $V_i'(\boldsymbol{x})$ have to be integrated over ϕ numerically since the relationship between Φ and ϕ is not straightforward for the three-dimensional case.

After applying the no-slip conditions (11a) to M_1 discrete points on S_p and applying the weighted averaging conditions (19c) to N_2 discrete rings on S_w- with M_2 weight functions chosen, we have (for $i = 1, 2, 3$)

$$\underbrace{\sum_{n=1}^{n} \sum_{m=0}}_{M_1 \text{ terms}} [B_{mn} B_{mn}^{(i)}(a, \theta_p, \Phi_p) + C_{mn} C_{mn}^{(i)}(a, \theta_p, \phi_p) + E_{mn} E_{mn}^{(i)}(a, \theta_p, \Phi_p)]$$

$$+ \frac{1}{8\pi} \sum_{n=2}^{N_2-1} \sum_{m=0}^{M_2-1} \sum_{j=1}^{3} \sum_{\alpha=1}^{3} f_{jm}(R_{n-2+\alpha})\, G_{ij}^{mn\alpha}(R_p, \phi_p, z_p) = V_i'^{(p)}(\theta_p, \Phi_p),$$

$$\text{at } \boldsymbol{x} = (a, \theta_p, \Phi_p) = (R_p, \phi_p, z_p) \in S_p, \quad p = 1, 2, 3, \ldots, M_1; \tag{20a}$$

$$\underbrace{\sum_{n=1}^{n} \sum_{m=0}}_{M_1 \text{ terms}} [B_{mn} B_{mnl}^{(i)}(R_q) + C_{mn} C_{mnl}^{(i)}(R_q) + E_{mn} E_{mnl}^{(i)}(R_q)]$$

$$+ \frac{1}{8\pi} \sum_{n=2}^{N_2-1} \sum_{j=1}^{3} \sum_{\alpha=1}^{3} \{f_{jl}(R_{n-2+\alpha})\, I_{ij}^{n\alpha}(R_q, l)\, \epsilon_{il} + f_{j,\,l+2}(R_{n-2+\alpha})$$

$$\times I_{ij}^{n\alpha}(R_q, l+2)\, \epsilon_{il}(1 - \omega_{l-M_2+2}) + f_{j,\,l-2}(R_{n-2+\alpha})\, I_{ij}^{n\alpha}(R_q, l-2)\, \omega_{l-2}\} = 0,$$

$$\text{for } q = 1, 2, 3, \ldots, N_2; \quad l = 0, 1, 2, \ldots, M_2 - 1; \quad (l \neq 0 \text{ when } i = 2). \tag{20b}$$

where

$$\epsilon_{il} = \begin{cases} 2 & \text{when } l = 0, \quad i = 1 \text{ or } 3; \\ 1 & \text{when } l \neq 0; \end{cases} \tag{20c}$$

$$\omega_s = \begin{cases} 0 & \text{when } s < 0, \\ 1 & \text{when } s \geqslant 0; \end{cases} \tag{20d}$$

$$I_{ij}^{n\alpha}(R, l) = A_\alpha^{(n)} g_{ij}^a(R; \hat{R}_{n-1}, \hat{R}_n; l, 3) + B_\alpha^{(n)} g_{ij}^b(R; \hat{R}_{n-1}, \hat{R}_n; l, 2)$$
$$+ C_\alpha^{(n)} g_{ij}^c(R; \hat{R}_{n-1}, \hat{R}_n; l, 1). \tag{20e}$$

Here $A_\alpha^{(n)}$, $B_\alpha^{(n)}$ and $C_\alpha^{(n)}$ are defined by (14); $\hat{R}_n$ by (13); g_{ij}^a, g_{ij}^b and g_{ij}^c by (17). In (20a, b), the Lamb series is truncated to M_1 terms. Note that $B_{0n}^{(i)}(r, \theta, \Phi) \equiv 0$ so that the sequence in which the terms are taken is $C_{01}, E_{01}, B_{11}, C_{11}, E_{11}, C_{02}, E_{02}, B_{12}, C_{12}, E_{12}, B_{22}, \ldots$. The term f_{20} does not appear since $\sin m\phi \equiv 0$ when $m = 0$. The $B_{mnl}^{(i)}(R_q)$, $C_{mnl}^{(i)}(R_q)$ and $E_{mnl}^{(i)}(R_q)$ represent the weighted integrals of $B_{mn}^{(i)}(a, \theta, \Phi)$, $C_{mn}^{(i)}(a, \theta, \Phi)$ and $E_{mn}^{(i)}(a, \theta, \Phi)$ over ϕ and have to be evaluated numerically:

$$B_{mnl}^{(i)}(R) = \int_0^{2\pi} B_{mn}^{(i)}(r, \theta, \Phi)\, w_{il}(\phi)\, \mathrm{d}\phi, \tag{20f}$$

$$C^{(i)}_{mnl}(R) = \int_0^{2\pi} C^{(i)}_{mn}(r, \theta, \Phi)\, w_{il}(\phi)\, \mathrm{d}\phi, \tag{20g}$$

$$E^{(i)}_{mnl}(R) = \int_0^{2\pi} E^{(i)}_{mn}(r, \theta, \Phi)\, w_{il}(\phi)\, \mathrm{d}\phi, \tag{20h}$$

where $(R, \phi, 0) = (r, \theta, \Phi)$ with $R = \text{const.}$ is a ring in the plane wall and $w_{il}(\phi)$ is given by (19d).

Equations (20a, b) constitute $N_T = 3M_1 + (3M_2 - 1)N_2$ equations, which can be solved for N_T unknowns: B_{mn}, C_{mn}, E_{mn} and $f_{jm}(R_q)$. The force and torque are then found from (10a, b).

3. Axisymmetric solutions

Solutions will be presented for two axisymmetric cases: (i) the sphere moving along the orifice axis in a quiescent fluid; (ii) Sampson's flow past a stationary sphere. Due to the axial symmetry, $F_x = T_y = 0$ in (2). To compare the results with Dagan *et al.* (1982b), we redefine the force correction factor for the axisymmetric cases as follows:

$$F_z = 6\pi\mu a(U_z F^{\mathrm{t}}_z + V_{z0} \tilde{F}^{\mathrm{s}}_z), \tag{21a}$$

where

$$V_{z0} = \frac{3q}{2\pi} \tag{21b}$$

is the flow velocity at the centre of the orifice opening.

On the sphere surface S_{p} the collocation points are selected according to the second scheme by Dagan *et al.* (1982b), i.e. for a given even number M_1, taking $\theta = (i-1)(180°/(M_1-2))$ for $i = 1, 2, \ldots, M_1 - 1$ and then replacing 0°, 90°, 180° by $0° + \delta$, $90° - \delta$, $90° + \delta$ and $180° - \delta$ to avoid the singularity of the coefficient matrix in (15a, b). On the plane wall $S_{\mathrm{w}}-$ the collocation points are unevenly placed so that the concentrated distribution near $R = 1.0$ may better describe the sharp changes in the wall stresses near the orifice edge. Extensive numerical tests were conducted for convergence of the solution as M_1, N_2, δ and R_{u} vary. It is found that (i) $\delta = 0.01°$ can secure convergence to five significant digits of both F^{t}_z and $\tilde{F}^{\mathrm{s}}_z$ for all spacings and radii; (ii) for most cases $M_1 = 6$–18 is sufficient to give five-digit accuracy, but for the worst case ($a = 10.0$, $z_0/a = 1.1$) $M_1 = 28$ can give only three-digit accuracy; (iii) for most cases $N_2 = 20$–30 can yield four- or five-digit accuracy, but for the same worst case $N_2 = 50$ can give only three digits; (iv) it is adequate to choose the truncation distance R_{u} as equal to twenty times either a or z_0, whichever is larger. The detailed tests are summarized in Yan (1985).

The truncation of the $S_{\mathrm{w}}-$ plane can be justified by the rapid decay of $f_z(\tilde{R})$ with the increase of $\tilde{R}$, as observed for a medium-sized sphere ($a = 0.5$) in figure 2. Remember that $f_z(\tilde{R})$ represents the normal stress difference across the plane wall due to the *disturbance* field $V'(y)$ (see (8a)). When the pressure difference $\Delta p = p_{-\infty} - p_{\infty} \neq 0$, the total normal stress difference across the wall is equal to the sum of $f_z(\tilde{R})$ and the normal stress difference due to Sampson's flow (in the absence of the sphere). For reference, the later for $\Delta p = 3.0$ is also plotted in the figure. Note that the presence of the sphere at different distances z_0 from the plane of the orifice opening induces different fluxes q through the orifice (Dagan *et al.* 1982b, p. 165). For the purpose of comparison, values of U (the translation velocity of the sphere) or Δp are chosen such that all the curves in figure 2 are presented for the same volumetric flux ($q = 1.0$). It is seen that when $\tilde{R}$ is large, $f_z(\tilde{R})$ decays in proportion to at least

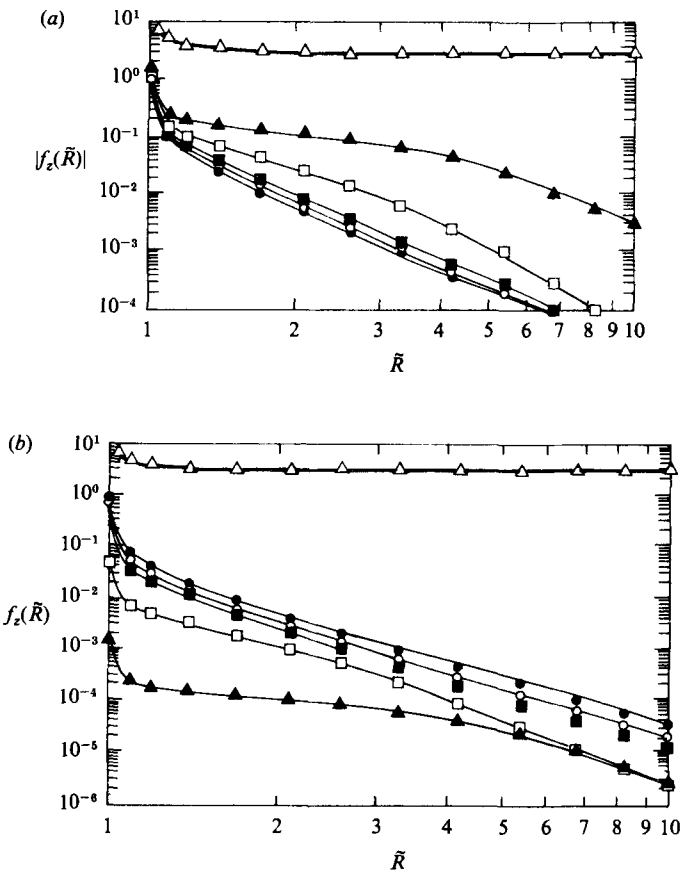

FIGURE 2. The typical $f_z(\tilde{R})$ for axisymmetric cases ($a = 0.5$). (*a*) Sphere moving in quiescent fluid: ●, $z_0/a = 1.1$ ($U = 0.75$); ○, 1.5 (0.87); ■, 2.0 (1.06); □, 4.0 (2.50); ▲, 10.0 (20.0); △, Sampson ($\Delta p = 3.0$, no sphere). (*b*) Sphere held fixed in Sampson's flow: ●, $z_0/a = 1.1$ ($\Delta p = 6.54$); ○, 1.5 (5.13); ■, 2.0 (4.22); □, 4.0 (3.17); ▲, 10.0 (3.00); △, Sampson ($\Delta p = 3.00$, no sphere).

the fourth power of $(1/\tilde{R})$. In either the case of a sphere moving in quiescent fluid or a sphere held fixed in Sampson's flow, the induced normal stress difference $|f_z(\tilde{R})|$ due to the *disturbance* of the sphere is several orders of magnitude smaller than the stress difference due to Sampson's flow for all values $\tilde{R} \geqslant 1.0$. When the sphere is held fixed in Sampson's flow, the singularity of the total normal stress at the orifice edge ($\tilde{R} = 1.0$) should behave essentially like that due to the Sampson flow alone, whose normal wall stress can be derived from (7*a*, *c*) as follows:

$$\tau_{zz} = \pm\frac{3q}{\pi}\left(\frac{1}{(\tilde{R}^2-1)^{\frac{1}{2}}}+\tan^{-1}(\tilde{R}^2-1)^{\frac{1}{2}}\right), \quad \text{when } \tilde{R} > 1.0, \quad z = 0. \tag{22}$$

When the sphere moves in quiescent fluid, although the local singularity of $f_z(\tilde{R})$ might not be adequately described by the piecewise quadratic interpolation in (14), the numerical results show that the substitution of (14) into the integral equations does yield the correct hydrodynamic force.

In tables 2 and 3, the force correction factors F_z^t and $\tilde{F}_z^s$ are compared with the solutions given by Dagan *et al.* (1982*b*) and by Davis (1983). Dagan *et al.* (1982*b*),

z_0/a		$a = 0.1$	$a = 0.5$	$a = 1.0$	$a = 5.0$	$a = 10.0$
10.0	(*a*)	−1.0723	−1.1246	−1.1259	−1.1251	−1.1253
	(*b*)	−1.0596	−1.1240	−1.1262	−1.1262	−1.1262
	(*c*)	−1.0730	−1.1248	−1.1259	−1.1261	—
5.0	(*a*)	−1.0666	−1.2638	−1.2814	−1.2850	−1.2822
	(*b*)	−1.0532	−1.2509	−1.2795	−1.2850	−1.2851
	(*c*)	−1.0667	−1.2618	−1.2804	−1.2837	—
2.0	(*a*)	−1.0540	−1.4264	−1.8654	−2.1194	−2.1250
	(*b*)	−1.0505	−1.3919	−1.8058	−2.1200	−2.1248
	(*c*)	−1.0542	−1.4843	−1.8396	−1.9981	—
1.5	(*a*)	−1.0523	−1.4205	−2.1042	−3.153	−3.185
	(*b*)	−1.0504	−1.3882	−2.0334	−3.1535	−3.1983
	(*c*)	−1.0526	−1.4872	−2.0863	−2.5059	—
1.1	(*a*)	−1.0513	−1.3946	−2.360	−8.47	−10.4
	(*b*)	−1.0503	−1.3777	−2.2867	−8.94	−10.5
	(*c*)	−1.0516	−1.4593	−2.2659	−2.8380	—

TABLE 2. The axisymmetric solution (comparison of F_z^t)
(*a*) the present work; (*b*) Dagan *et al.* (1982*b*); (*c*) Davis (1983).

z_0/a		$a = 0.1$	$a = 0.5$	$a = 1.0$	$a = 5.0$	$a = 10.0$
10.0	(*a*)	0.53439	0.043079	0.011102	0.00044801	0.00011204
	(*b*)	0.52797	0.043026	0.011094	0.00044814	0.00011207
	(*c*)	0.53485	0.043220	0.011139	0.0004499	—
5.0	(*a*)	0.84852	0.17298	0.049182	0.0020527	0.0005126
	(*b*)	0.83796	0.16986	0.048597	0.0020285	0.00050774
	(*c*)	0.84824	0.17554	0.050131	0.0020924	—
2.0	(*a*)	1.0069	0.65155	0.3593	0.0222	0.00565
	(*b*)	1.0036	0.62720	0.32754	0.022291	0.0056546
	(*c*)	1.0068	0.70094	0.45763	0.030870	—
1.5	(*a*)	1.0224	0.79839	0.568	0.069	0.018
	(*b*)	1.0206	0.77576	0.48320	0.0863	0.0185
	(*c*)	1.0225	0.81957	0.82430	0.10522	—
1.1	(*a*)	1.0319	0.91163	0.753	0.24	0.20
	(*b*)	1.0310	0.90571	0.64018	0.191	0.149
	(*c*)	1.0321	0.88548	1.0681	0.42048	—

TABLE 3. The axisymmetric solution (comparison of F_z^s)
(*a*) the present work; (*b*) Dagan *et al.* (1982*b*); (*c*) Davis (1983).

using the multipole-series technique, satisfied the no-slip conditions exactly through analytic methods on S_w- and numerically through the collocation method on S_p, whereas in the present work we have used the collocaton method on both the boundaries. Therefore, in principle, the former should be more accurate. The present results differ from those of Dagan *et al.* by one to a few percent for most of the cases in the tables, a reasonable accuracy for the integral-equation method in general. The solution by Davis was obtained for a Stokeslet and can be taken as an approximation for a small sphere, correct to a^3. It is seen in the tables that the results by Davis,

z_0/a	$a = 0.1$	$a = 0.25$	$a = 0.5$	$a = 0.75$	$a = 1.0$
1.1	−1.0513	−1.1448	−1.3946	−1.9234	−2.360
1.0	−1.0511	−1.1424	−1.3856	−1.9438	−2.457
0.5	−1.0503	−1.1327	−1.3364	−1.9163	−3.332
0.1	−1.0501	−1.1307	−1.3116	−1.8194	−10
0.05	−1.0501	−1.1305	−1.3107	−1.7888	—
0.0	−1.0501	−1.1291	−1.3104	−1.7768	—

TABLE 4. The axisymmetric solution (results of F_z^t for $z_0/a \leqslant 1.1$)

z_0/a	$a = 0.1$	$a = 0.25$	$a = 0.5$	$a = 0.75$	$a = 1.0$
1.1	1.0319	1.0209	0.91163	0.8082	0.753
1.0	1.0338	1.0314	0.93779	0.8964	0.794
0.5	1.0408	1.0705	1.0460	1.0531	0.957
0.1	1.0431	1.0837	1.0888	1.230	1.2
0.05	1.0431	1.0842	1.0903	1.249	—
0.0	1.0431	1.0843	1.0908	1.255	—

TABLE 5. The axisymmetric solution (results of $\tilde{F}_z^s$ for $z_0/a \leqslant 1.1$)

while having a comparable accuracy with ours for small particles ($a \leqslant 1.0$), deteriorates with the increase of the sphere radius a as the orifice is approached.

Although the solutions by Dagan *et al.* (1982*b*) are more accurate in principle, their range of validity is limited to $z_0/a \geqslant 1.1$ only. Their method cannot treat the case in which the sphere intersects the orifice opening. The latter case is important in treating pore-entrance phenomena such as the fine structure of osmosis at a pore entrance (Yan *et al.* 1986) and the collection efficiency of particles in nucleopore filters (Wang *et al.* 1986). The latter may be critically dependent on the values of F_z^t and $\tilde{F}_z^s$ in the immediate vicinity of the pore opening. Our present method applies to this case without difficulty. In tables 4 and 5 typical results for the force correction factors F_z^r and $\tilde{F}_z^s$ are presented for $0 \leqslant z_0/a \leqslant 1.1$. The different significant digits reflect the different accuracy of convergence. No convergence is reached within reasonable computation efforts for $a = 1.0$ and $z_0/a \leqslant 0.05$ (i.e. almost choking of the orifice opening by the sphere).

The neutrally buoyant velocity of a sphere carried by the flow towards the pore can be obtained by requiring a zero drag force on the sphere, i.e. $F_z = 0$ in (21*a*). Then

$$\frac{U_z}{V_{z0}} = -\frac{\tilde{F}_z^s}{F_z^t}. \tag{23}$$

The results from this equation are plotted for $z_0/a = 0$–1.1 in figure 3. At $z_0/a = 1.1$ the present solution matches that by Dagan *et al.* (1982*b*), as shown by the arrowheads on the right side of the figure. For comparison, the figure also indicates the zero-drag velocity of a sphere carried axisymmetrically by the flow in an infinite circular cylindrical tube (Haberman & Sayre 1958), shown by the arrowheads on the left side. It is evident that the present results for $z_0 = 0$ are quite close to these limiting values, in spite of our neglecting the pore length. This confirms our earlier conjecture that the pore length itself has only a minor effect on the sphere–pore entrance interaction.

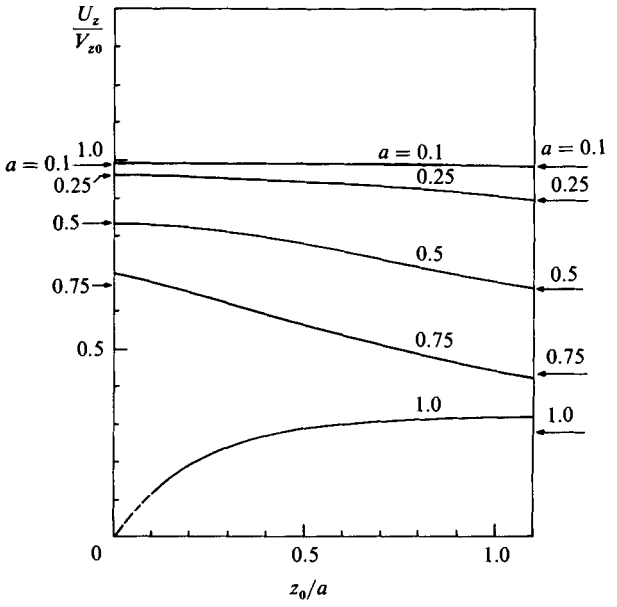

FIGURE 3. The neutrally buoyant velocity of the sphere, $0 \leqslant z_0/a \leqslant 1.1$, axisymmetric cases: ——, present work; – – –, extrapolation; ⟶, Haberman & Sayre (1958); ⟵, Dagan *et al.* (1982*b*).

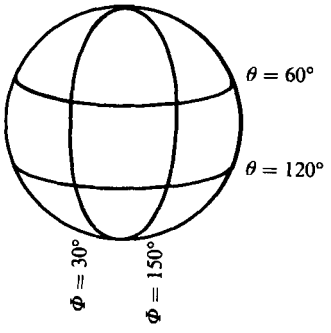

FIGURE 4. The collocaton points on the sphere surface for the three-dimensional case.

4. Three-dimensional solutions

For most of our three-dimensional calculations the number of collocation points on the sphere surface S_p was chosen as $M_1 = 4$ and the position of points was selected as shown in figure 4, according to Ganatos *et al.* (1978). The number of collocation rings on the plane wall $S_w -$ was chosen to lie in the range of $N_2 = 10$–18. The practical consideration of the computation time and accuracy has restricted $M_2 \leqslant 8$ in our calculations. With $M_1 = 4$, $M_2 = 8$ and $N_2 = 10$, the number of simultaneous equations to be solved is $N_T = 242$. One run with this value of N_T requires 16 minutes of CPU time on an IBM 3081 computer and a memory of 683 KB.

There were previously no three-dimensional solutions for the twelve hydrodynamic coefficients in (2) for a finite particle near an orifice. Miyazaki & Hasimoto (1984) derived a solution for a translating Stokeslet near an orifice, which can be used as an

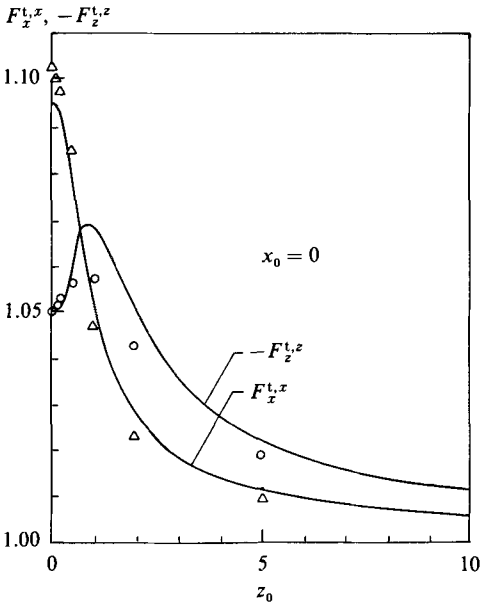

FIGURE 5. Comparison of results along the orifice axis ($x_0 = 0$) between the present solution (○, $-F_z^{t,z}$; △, $F_x^{t,x}$) and Miyazaki & Hasimoto (1984) (——).

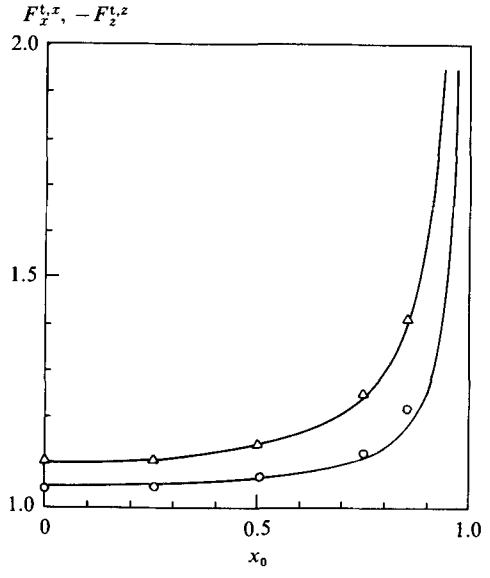

FIGURE 6. Comparison of results at the orifice opening ($z_0 = 0$) between the present solution and Miyazaki & Hasimoto (1984). Symbols as figure 5.

approximation for a small particle, correct to the order of the particle radius a. In figures 5 and 6, the present solutions for both $F_x^{t,x}$ and $F_z^{t,z}$ for $a = 0.1$ are compared with those by Miyazaki & Hasimoto for either $x_0 = 0$ (along the orifice axis) or $z_0 = 0$ (at the orifice opening). The agreement is very good.

Numerical tests for the convergence were conducted for a wide range of M_1, M_2 and

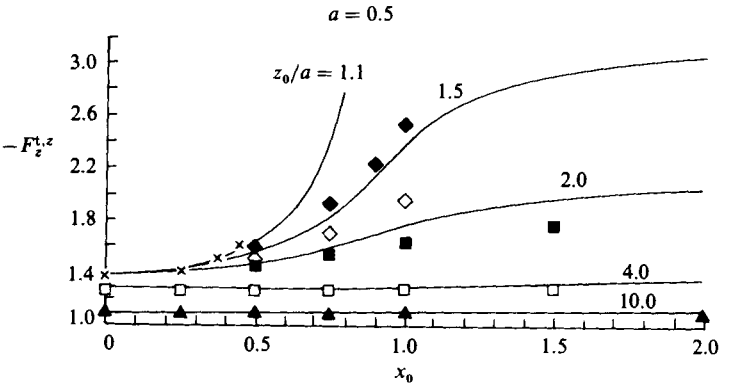

FIGURE 7. The results for $F_z^{t,z}$, the three-dimensional cases, $a = 0.5$. ×, $z_0/a = 0$; △, 0.5; ◆, 1.1; ◇, 1.5; ■, 2.0; □, 4.0; ▲, 10.0.

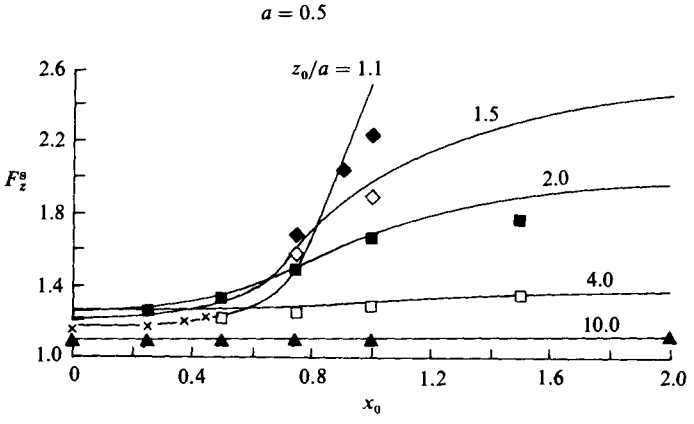

FIGURE 8. The results for F_z^s, the three-dimensional cases, $a = 0.5$. Symbols as figure 7.

N_2 (the details can be found in Yan 1985). To secure the convergence, the required number M_2 of harmonics increases as the sphere goes outward from the orifice axis. When the sphere centre is within a few orifice radii of the orifice axis and not very close to the plane wall S_w-, convergence to at least three significant digits was reached for the four major correction factors ($F_x^{t,x}$, $F_z^{t,z}$, $\tilde{F}_z^s$ and T_y^r) and to at least two digits for the rest of the factors, which are by themselves small. However, when the wall S_w- was approached, the convergence deteriorated. This is because the description of the very rapid change in stresses for the small *local* area of the thin lubrication layer requires very high-order (M_2) harmonics when the sphere–wall spacing is small.

Restricted by excessive computation time, accurate three-dimensional solutions are presented only for a medium size sphere ($a = 0.5$). These solutions are valid in a region not far off-axis and not very close to the orifice wall. Despite the above limitations, these solutions for a finite particle provide insight into the three-dimensional spatial variation of all the twelve force and torque correction factors as defined in (2). The region of validity of these solutions is of primary importance for many pore-entrance phenomena that could not be treated by the earlier approximate theory of Dagan *et al.* (1983). Based on an analysis of the behaviour of these

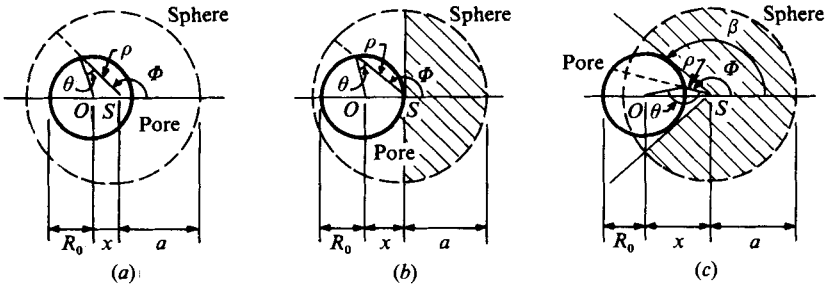

FIGURE 9. Three cases of the sphere-to-orifice relative positions. (*a*) $0 \leqslant x < R_0$; (*b*) $x = R_0$; (*c*) $x > R_0$.

			F^t_{z0}			
z_0/a	$a/R_0 = 0.1$	$a/R_0 = 0.5$	$a/R_0 = 1.0$	$a/R_0 = 5.0$	$a/R_0 = 10.0$	$a/R_0 = \infty$
1.1	−1.0503	−1.3777	−2.2867	−8.94	−10.5	−11.4592
1.5	−1.0504	−1.3882	−2.0334	−3.1535	−3.1983	−3.2054
2.0	−1.0505	−1.3919	−1.8058	−2.1200	−2.1248	−2.1255
4.0	−1.0519	−1.3091	−1.3655	−1.3801	−1.3802	−1.3802
10.0	−1.0596	−1.1240	−1.1262	−1.1262	−1.1262	−1.1262
∞	−1.0000	−1.0000	−1.0000	−1.0000	−1.0000	−1.0000

		F^s_{z0}			
z_0/a	$a/R_0 = 0.1$	$a/R_0 = 0.5$	$a/R_0 = 1.0$	$a/R_0 = 5.0$	$a/R_0 = 10.0$
1.1	1.0435	1.1797	1.4148	5.97	18.2
1.5	1.0436	1.2121	1.5704	3.91	4.18
2.0	1.0437	1.2544	1.6377	2.2514	2.2675
4.0	1.0457	1.2693	1.3435	1.3623	1.3625
10.0	1.0559	1.1187	1.1205	1.1208	1.1208
∞	1.0000	1.0000	1.0000	1.0000	1.0000

TABLE 6. The axisymmetric solutions F^t_{z0} and F^s_{z0}

Sources: F^t_{z0} for $a/R_0 = \infty$, Brenner (1961). All others, Dagan *et al.* (1982*b*).

numerical solutions, we are able to propose reasonable interpolation formulas, which can be applied over a wide range of particle sizes and for an arbitrary particle positon outside the orifice.

In figures 7 and 8, the accurate numerical results for $F^{t,z}_z$ and F^s_z are denoted by different symbols for the range $z_0/a = 0$–10 and $a = 0.5$. Here F^s_z is defined as $F^s_z = (V_{z0}/V^S_z)\,\tilde{F}^s_z$ for convenient comparison with other solutions, and V_{z0} and V^S_z are given by (21*b*) and (7*b*) respectively. In these and the following figures, the symbols are plotted only for the range of x_0 where our solutions converge well within the selected values of M_1, M_2 and N_2. The solid lines in these figures represent the approximate interpolations using known solutions for the axisymmetric motion of a sphere near an orifice or a disk (Dagan *et al.* 1982*b*; Dagan, Pfeffer & Weinbaum 1982). The interpolation technique was proposed by Yan *et al.* (1986) and is described in detail in Yan (1985). As shown in figure 9, three cases are considered with the projection S of the sphere centre lying (*a*) inside, (*b*) on the edge and (*c*) outside the orifice. In case (*a*), the local radius ρ from S to the pore edge varies with angle Φ. The axisymmetric values of F^t_{z0} and F^s_{z0}, as summarized in table 6 (as functions of

F^{t}_{zc}

z_0/a	$a/R_c = 0.0$	$a/R_c = 0.1$	$a/R_c = 0.5$	$a/R_c = 1.0$	$a/R_c = 5.0$	$a/R_c = 10.0$
1.1	−11.4592	−11.4593	−11.559	−11.784	−3.04	−1.56
1.5	−3.2054	−3.2055	−3.2952	−3.0812	−1.2643	−1.1046
2.0	−2.1255	−2.1258	−2.1798	−1.8936	−1.1354	−1.0620
4.0	−1.3802	−1.3818	−1.3272	−1.1848	−1.0350	−1.0172
10.0	−1.1262	−1.1305	−1.0563	−1.0287	−1.0057	−1.0028
∞	−1.0000	−1.0000	−1.0000	−1.0000	−1.0000	−1.0000

F^{s}_{zc}

z_0/a	$a/R_c = 0.1$	$a/R_c = 0.5$	$a/R_c = 1.0$	$a/R_c = 5.0$	$a/R_c = 10.0$
1.1	3.4562	3.7436	3.4298	1.3188	1.1301
1.5	2.5511	2.6614	2.2719	1.2141	1.1008
2.0	2.0315	2.0418	1.7207	1.1344	1.0467
4.0	1.4080	1.3239	1.1850	1.0361	1.0178
10.0	1.1350	1.0570	1.0291	1.0058	1.0029
∞	1.0000	1.0000	1.0000	1.0000	1.0000

TABLE 7. The axisymmetric solutions F^{t}_{zc} and F^{s}_{zc}
Sources: F^{t}_{zc} for $a/R_c = 0$, Brenner (1961). All others, Dagan *et al.* (1982).

the ratio a/R_0 of the sphere to pore radii), are averaged over Φ and these average values are taken as our approximation. That is

$$F^{t,z}_{z} = \frac{1}{\pi}\int_0^{\pi} F^{t}_{z0}\left(\frac{a}{\rho}\right)\mathrm{d}\Phi, \quad F^{s}_{z} = \frac{1}{\pi}\int_0^{\pi} F^{s}_{z0}\left(\frac{a}{\rho}\right)\mathrm{d}\Phi. \tag{24}$$

In case (*b*), for the range of $0 \leqslant \Phi \leqslant \frac{1}{2}\pi$, the sphere sees a disk of infinite size rather than an orifice. Therefore the axisymmetric solutions F^{t}_{zc} and F^{s}_{zc} for a sphere near a disk, as summarized in table 7 (as functions of the ratio a/R_c of the sphere to disc radii), are used for this range of Φ in the averaging process, namely

$$\left.\begin{aligned} F^{t,z}_{z} &= \tfrac{1}{2}[F^{t}_{z2} + F^{t}_{zc}(a/R_c = 0)], \\ F^{s}_{z} &= \tfrac{1}{2}[F^{s}_{z2} + F^{s}_{zc}(a/R_c = 0)], \end{aligned}\right\} \tag{25}$$

where

$$F^{t}_{z2} = \frac{2}{\pi}\int_{\frac{1}{2}\pi}^{\pi} F^{t}_{z0}(a/\rho)\,\mathrm{d}\Phi, \quad F^{s}_{z2} = \frac{2}{\pi}\int_{\frac{1}{2}\pi}^{\pi} F^{s}_{z0}(a/\rho)\,\mathrm{d}\Phi. \tag{26}$$

In case (*c*), the sphere sees a disk of $R_c = \infty$ for $0 \leqslant \Phi \leqslant \beta$ and a disk of radius ρ for $\beta < \Phi \leqslant \pi$. However, for $\beta < \Phi \leqslant \pi$ the solid wall beyond the far edge of the orifice cannot be ignored. To account for this, we give the orifice effect, F^{t}_{z2} or F^{s}_{z2} as evaluated in (26), a weight of R_0/x and the disk effect, as averaged over $\beta < \Phi \leqslant \pi$, a weight of $(1 - R_0/x)$. Here x is the distance between point S and the orifice centre O (figure 9). Thus,

$$\left.\begin{aligned} F^{t}_{z} &= \frac{1}{\pi}\left[\beta F^{t}_{zc}(a/R_c = 0) + (\pi-\beta)\frac{R_0}{x}F^{t}_{z2} + \left(1-\frac{R_0}{x}\right)\int_{\beta}^{\pi} F^{t}_{zc}\left(\frac{a}{\rho}\right)\mathrm{d}\Phi\right], \\ F^{s}_{z} &= \frac{1}{\pi}\left[\beta F^{s}_{zc}(a/R_c = 0) + (\pi-\beta)\frac{R_0}{x}F^{s}_{z2} + \left(1-\frac{R_0}{x}\right)\int_{\beta}^{\pi} F^{s}_{zc}\left(\frac{a}{\rho}\right)\mathrm{d}\Phi\right]. \end{aligned}\right\} \tag{27}$$

Interpolation formulas (24)–(27) yield correct limiting values when $x_0 \to \infty$. As can be seen in figures 7 and 8, the interpolations (solid lines) agree reasonably with the

	$-F^{t,x}_{x0}$				$-F^{t,x}_{x\infty}$ (Goldman *et al.* 1967)
z_0/a	$a = 0.1$	$a = 0.5$	$a = 1.0$	$a = 5.0$	
10.0	1.05	1.05	1.05	1.05	1.06
4.0	1.09	1.13	1.13	1.13	1.15
2.0	1.10	1.29	1.30	1.30	1.42
1.5	1.10	1.39	1.44	1.45	1.63
1.1	1.10	1.50	1.69	1.78	2.32
	$-T^{r}_{y0}$				$-T^{r}_{y\infty}$ (Goldman
z_0/a	$a = 0.1$	$a = 0.5$	$a = 1.0$	$a = 5.0$	*et al.* 1967)
10.0	1.00	1.00	1.00	1.00	1.00
4.0	1.00	1.00	1.00	1.00	1.01
2.0	1.00	1.01	1.02	1.02	1.06
1.5	1.00	1.01	1.03	1.06	1.13
1.1	1.00	1.01	1.06	1.15	1.49
	$-F^{r}_{x0}$				$-F^{r}_{x\infty}$ (Goldman
z_0/a	$a = 0.1$	$a = 0.5$	$a = 1.0$	$a = 5.0$	*et al.* 1967)
10.0	0.0008	0.0013	0.0013	0.0013	0.0000
4.0	0.0013	0.0086	0.0090	0.0090	0.0090
2.0	0.0008	0.0290	0.0414	0.0452	0.0092
1.5	0.0007	0.0417	0.0774	0.0977	0.0229
1.1	0.0005	0.0510	0.1536	0.2573	0.1270

TABLE 8. The axisymmetric and far-field values of $F^{t,x}_x$, T^r_y and F^r_x

accurate numerical results (symbols) for $a = 0.5$. Thus, it confirms the plausibility of the interpolation used The interpolation formulas presented herein can be applied for particle sizes in the range $0.1 \leqslant a \leqslant 10.0$ and for an arbitrary particle positon for $z_0/a \geqslant 1.1$.

For $F^{t,x}_x$ and T^r_y we cannot use the interpolation technique just described because the corresponding axisymmetric solutions for a sphere near a finite disk are not available. However, it is found that the accurate numerical results for $a = 0.5$ may be well approximated by the following formulas:

$$\left.\begin{aligned} F^{t,x}_x &= (F^{t,x}_{x\infty} - F^{t,x}_{x0})\left[1 - \operatorname{sech}\left(0.6\,\frac{x}{(z_0/a)^{\frac{1}{3}}}\right)\right] + F^{t,x}_{x0}, \\ T^r_y &= (T^r_{y\infty} - T^r_{y0}\left[1 - \operatorname{sech}\left(0.8\,\frac{X}{(z_0/a)^{\frac{1}{4}}}\right)\right] + T^r_{y0}. \end{aligned}\right\} \tag{28}$$

where the subscript 0 denotes the axisymmetric value for a sphere near an orifice, which is calculated by the present method, and the subscript ∞ denotes the far-field value for a sphere near an infinite solid plane wall (Goldman, Cox & Brenner 1967). Both these values are given for $z_0/a = 1.1$–10.0 and $a = 0.1$–5.0 in table 8. The approximate results for $a = 0.5$ using these formulas are plotted by lines in figures 10 and 11 with the symbols denoting the accurate numerical solutions. The very close agreement for $a = 0.5$ suggests that (27) might be useful also for other particle sizes since the limiting values $F^{t,x}_{x0}$, $F^{t,x}_{x\infty}$ etc. have taken into consideration the effect of the particle size, as shown in table 8.

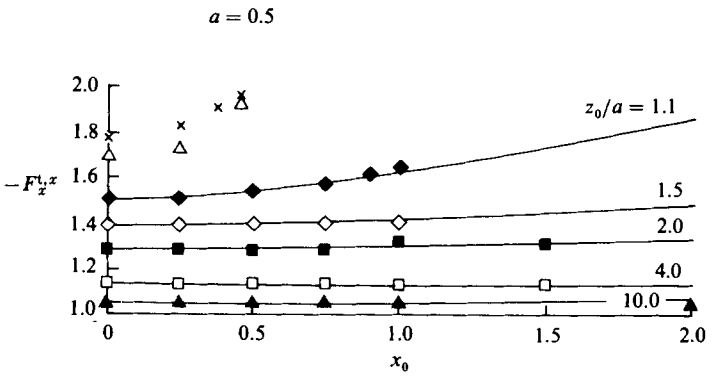

FIGURE 10. The results for $F_x^{t,x}$, the three-dimensional cases, $a = 0.5$. Symbols as figure 7.

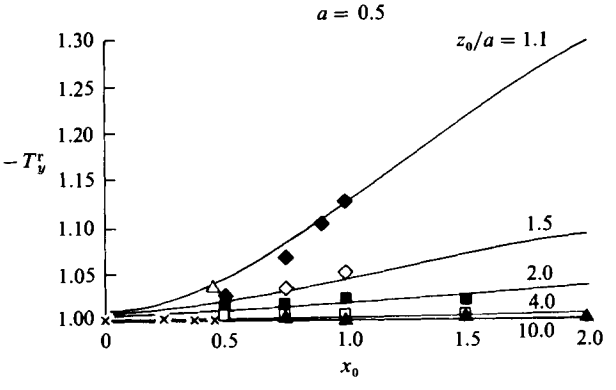

FIGURE 11. The results for T_y^r, the three-dimensional cases, $a = 0.5$. Symbols as figure 7.

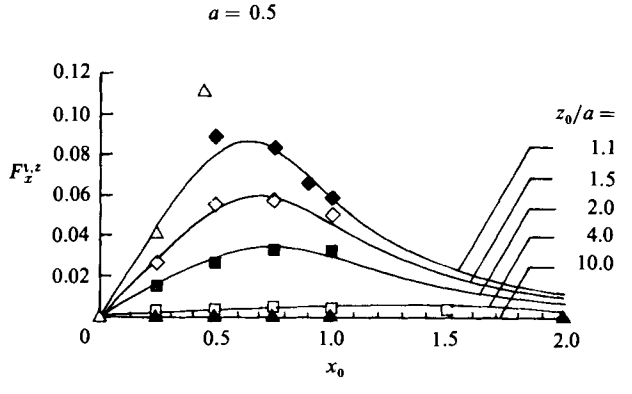

FIGURE 12. The results for $F_x^{t,z}$, the three-dimensional cases, $a = 0.5$. Symbols as figure 7.

Comparison of figures 7 and 8 with figures 10 and 11 shows that while $F_z^{t,z}$ and F_z^s change substantially between the axisymmeytric values for $x_0 = 0$ and the far-field solutions for large x_0, $F_x^{t,x}$ and T_y^r are relatively insensitive to the radial position x_0 of the sphere centre. This can be explained by the fact that the translation normal to the wall or the Sampson flow induces a much larger flow through the orifice than the translation parallel to the wall or the rotation so that the presence of the orifice opening has a greater influence on $F_z^{t,z}$ and F_z^s.

z_0/a	$a = 0.1$	$a = 0.5$	$a = 1.0$	$a = 5.0$
		$F_{x1}^{t,z}$		
10.0	0.0023	0.0000	0.0000	0.0000
4.0	0.0055	0.0016	0.0001	0.0000
2.0	0.0039	0.0144	0.0026	0.0000
1.5	0.0031	0.0266	0.0060	0.0003
1.1	0.0024	0.0413	0.0096	0.0017
		$-F_{z1}^{r}$		
10.0	0.0001	0.0000	0.0000	0.0000
4.0	0.0006	0.0003	0.0001	0.0000
2.0	0.0008	0.0035	0.0024	0.0000
1.5	0.0009	0.0061	0.0092	0.0002
1.1	0.0009	0.0092	0.0324	0.0014
		$\tilde{F}_{x1}^{s}$		
10.0	0.061	0.002	0.000	0.000
4.0	0.076	0.018	0.003	0.000
2.0	0.049	0.051	0.010	0.000
1.5	0.038	0.064	0.011	0.000
1.1	0.029	0.072	0.010	0.000
		$-\tilde{T}_{y1}^{s}$		
10.0	0.006	0.000	0.000	0.000
4.0	0.018	0.005	0.001	0.000
2.0	0.022	0.025	0.011	0.000
1.5	0.023	0.035	0.022	0.000
1.1	0.024	0.046	0.035	0.001

TABLE 9. The values of $F_x^{t,z}$, F_z^r, $\tilde{F}_x^s$ and $\tilde{T}_y^s$ at $x_0 = 0.25$

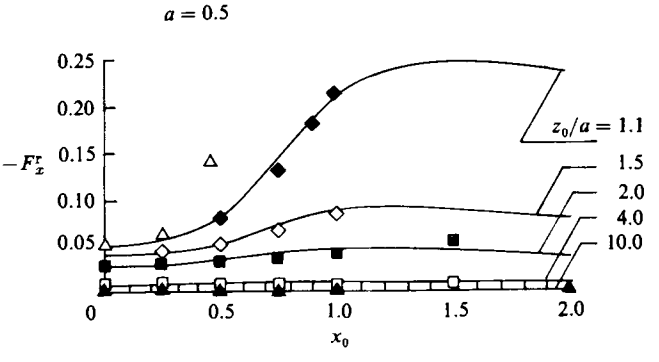

FIGURE 13. The results for F_x^r, the three-dimensional cases, $a = 0.5$. Symbols as figure 7.

Our numerical solutions show that $F_z^{t,z}$, F_z^s, $F_x^{t,x}$ and T_y^r are of the order of unity whereas the others are one order of magnitude smaller. The accurate numerical results for $F_x^{t,z}$ are presented for $a = 0.5$ and $z_0/a = 1.1$–10.0 by symbols in figure 12 with the solid lines denoting the approximate interpolation formula

$$F_x^{t,z} = \frac{[0.473(z_0/a)+0.0172]\,F_{x1}^{t,z}\,x}{x^4+0.43(z_0/a)}. \tag{29}$$

where $F_{x1}^{t,z}$ represents the value of $F_x^{t,z}$ at $x_0 = 0.25$. The values for $F_{x1}^{t,z}$ for $a = 0.1$–5.0

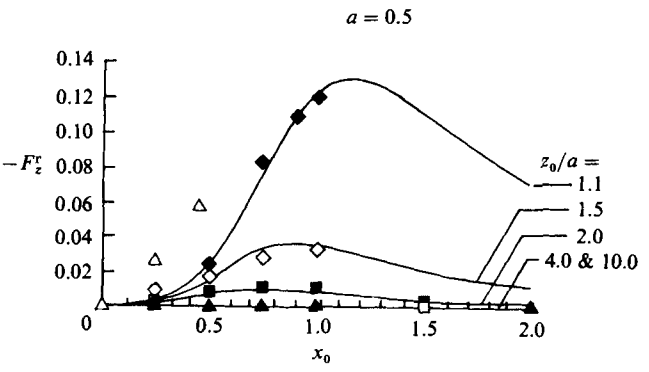

FIGURE 14. The results for F_z^r, the three-dimensional cases, $a = 0.5$. Symbols as figure 7.

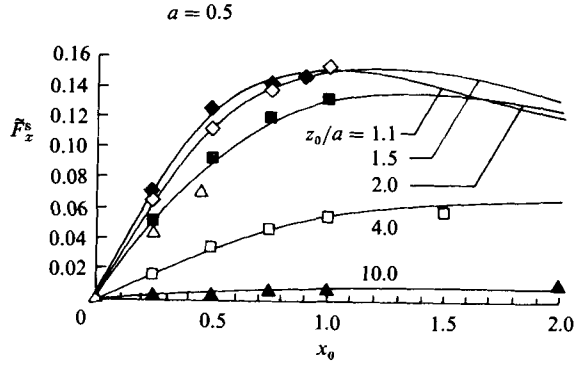

FIGURE 15. The results for $\tilde{F}_x^s$, the three-dimensional cases, $a = 0.5$. Symbols as figure 7.

are given in table 9. This hydrodynamic coefficient represents the cross-coupling effect, i.e. the lateral force in the x-direction generated by the sphere translation in the z-direction. When the sphere is located at the orifice axis ($x_0 = 0$) or far away from the orifice ($x_0 \to \infty$), $F_x^{t,z}$ vanishes. It is seen from the figure that $F_x^{t,z}$ is negligible everywhere except in the immediate vicinity of the orifice edge ($x_0 \approx 1.0$ and $z_0 \approx 1.0$).

Figures 13 and 14 show the effects of the sphere rotation on the force components in the x- and z-directions respectively. The accurate numerical results (symbols) for $a = 0.5$ and $z_0/a = 0.5$–10.0 are well approximated by the interpolation formulas (solid lines)

$$\left.\begin{aligned} F_x^r &= F_{x\infty}^r + \frac{0.30(z_0/a)^{-2.5}x^3 + F_{x0}^r - F_{x\infty}^r}{x^4+1}, \\ F_z^r &= \frac{(49.536(z_0/a)^{-4.5} + 0.0225)F_{z1}^r x^3}{x^5 + 2.15(z_0/a)^{-4.5}}, \end{aligned}\right\} \tag{30}$$

where the subscript 0 denotes the axisymmetric value for a sphere near an orifice ($x_0 = 0$) and subscript ∞ the far-field value for a sphere near an infinite solid plane wall. The subscript 1 again denotes the value at $x_0 = 0.25$. F_{x0}^r and $F_{x\infty}^r$ are listed in table 8 and F_{z1}^r in table 9, for $a = 0.1$–5.0 and $z_0/a = 1.1$–10.0. Here $F_{x\infty}^r$ is taken from Goldman *et al.* (1967) and the other coefficients are calculated using the present numerical method. It is observed from these figures that the interpolation curves for F_x^r approach the correct limiting values when $x_0 \to 0$ or $x_0 \to \infty$ and F_x^r is insignificant

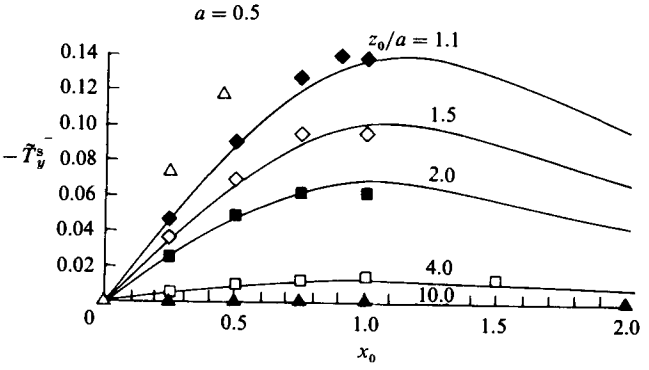

FIGURE 16. The results for $\tilde{T}^s_y$, the three-dimensional cases, $a = 0.5$. Symbols as figure 7.

except in the neighbourhood of the orifice wall ($z_0/a \approx 1.0$); one also observes that F^r_z vanishes when $x_0 \to 0$ or $x_0 \to \infty$ and it is negligible except in the immediate vicinity of the orifice edge ($z_0/a \approx 1.0$ And $x_0 \approx 1.0$).

Figures 15 and 16 show the effects of the flow through the orifice on the force and torque exerted on a stationary sphere. The accurate numerical results (symbols) for $a = 0.5$ and $z_0 = 0.5$–10.0 are well approximated by the interpolation formulas (solid lines)

$$\left.\begin{aligned} \tilde{F}^s_x &= \frac{[3.6(z_0/a)^{0.9}+0.225]\,\tilde{F}^s_{x1}\,x}{x^2+0.9(z_0/a)^{0.9}}, \\ \tilde{T}^s_y &= \frac{[12(z_0/a)^{-\frac{1}{2}}+0.0625]\,\tilde{T}^s_{y1}\,x}{x^3+3(z_0/a)^{-\frac{1}{2}}}, \end{aligned}\right\} \tag{31}$$

where the subscript 1 denotes the value at $x_0 = 0.25$ and $\tilde{F}^s_{x1}$ and $\tilde{T}^s_{y1}$ are presented for $a = 0.1$–5.0 and $z_0/a = 1.1$–10.0 in table 9. It is seen from these figures that both $\tilde{F}^s_x$ and $\tilde{T}^s_y$ vanish when $x_0 \to 0$ or $x_0 \to \infty$ and they are insignificant except near the orifice edge ($x_0 \approx 1.0$ and $z_0/a \approx 1.0$).

The rest of the twelve force and torque correction factors can be found through the reciprocal theorem (Happel & Brenner 1973, p. 85) as follows:

$$F^{t,x}_z = F^{t,z}_x, \quad T^{t,x}_y = \tfrac{3}{4}F^r_x, \quad T^{t,z}_y = \tfrac{3}{4}F^r_z. \tag{32}$$

In conclusion, all the interpolation curves presented herein agree remarkably well with the accurate numerical solutions for $a = 0.5$ in the range of validity of these solutions. The interpolation curves approach correct limiting values when $x_0 \to 0$ or $x_0 \to \infty$ and also account for the effect of the particle size through the coefficient values given in tables 6–9. Therefore, one can reasonably assume that (24)–(31) provide good approximations for a wide range of particle sizes when $z_0/a \geqslant 1.1$. Since these interpolations require very little computation time and no other approximate solutions are presently available, the techniques presented herein should be of practical value.

5. Concluding remarks

In this paper we have proposed a combined multipole series representation and integral-equation method to treat the problem of hydrodynamic interaction of a

finite sphere with the entrance geometry of a zero-thickness orifice. This combined method takes advantage of the flexibility of the integral-equation method in treating a complicated geometry and reduces its disadvantages of lower accuracy and greater computation time by using the multipole series representation for the disturbance on the sphere. This combined approach provides a very substantial improvement in accuracy and computational time over a direct numerical solution of the integral equation (8) provided the velocity has a smooth distribution on the sphere surface (see footnote §2.2).

For the axisymmetric case, the present method has successfully treated the difficult case of a finite sphere intersecting the plane of the orifice opening, which could not be treated by previous methods. For the three-dimensional case, the first accurate numerical solutions have been obtained for the twelve force and torque correction factors for a medium sized sphere at an arbitrary position within a few orifice radii from the orifice axis and not very close to the wall. Based on these solutions, approximate interpolation techniques have been developed, which can be used for the entire flow field for $z_0/a \geqslant 1.1$ and for a wide range of particle sizes. This greatly enhances the usefulness of the present solutions.

The purpose of the present work is to evaluate the hydrodynamic force and torque on the sphere in the presence of the orifice. Restricted by the excessive computation cost, the lower-order harmonics cannot adequately describe the details in the thin lubrication layer (when the sphere is very close to the orifice wall) or the local singular behaviour of the stresses at the orifice edge. However, the induced stresses due to the disturbance of the sphere proved to be several orders of magnitude smaller than those due to Sampson's flow in the absence of the particle and the present scheme proved to yield correct results for the hydrodynamic force and torque.

Because of its flexibility, the combined method proposed herein is a very promising technique for treating more complicated geometries, such as the entrance of a particle into a finite-length pore or the entrance problem for a periodic array of pores. Two important considerations in any attempt to improve the present method will be how to increase the accuracy and how to reduce the computation time.

The authors wish to thank the National Science Foundation for supporting this research under grant ENG82-00301 and The City University of New York, Computer Center for the use of their facilities. The helpful discussions with Professors R. Skalak and A. Silberberg are appreciated. This work has been performed in partial fulfillment of the requirements for the Ph.D. degree of Z. Yan from the School of Engineering of The City College of The City University of New York.

Appendix. The evaluations of $H_{ij}^{(\beta)}(R, \phi, z; b_1, b_2; m)$

If all the variables in (16*c*), defining $H_{ij}^{(\beta)}(R, \phi, z; b_1, b_2; m)$, are written in the cylindrical coordinates $(\tilde{R}, \tilde{\phi}, \tilde{z})$, the inner integrals over $\tilde{\phi}$ can be expressed in terms of the following integrals:

$$\left.\begin{aligned} C_0(l,p,A,B,\phi) &= \int_0^{2\pi} \frac{\cos l\tilde{\phi}\,\mathrm{d}\tilde{\phi}}{[A^2-B^2\cos(\tilde{\phi}-\phi)]^{p/2}}, \\ S_0(l,p,A,B,\phi) &= \int_0^{2\pi} \frac{\sin l\tilde{\phi}\,\mathrm{d}\tilde{\phi}}{[A^2-B^2\cos(\tilde{\phi}-\phi)]^{p/2}}, \end{aligned}\right\} \tag{A 1}$$

where $l = m-2, m-1, m, m+1, m+2$, $p = 1, 3$; A and B are given by

$$\left.\begin{aligned} A^2 &= \tilde{R}^2 + R^2 + z^2, \\ B^2 &= 2\tilde{R}R. \end{aligned}\right\} \tag{A 2}$$

Here (R, ϕ, z) is a fixed field point and $(\tilde{R}, \tilde{\phi}, \tilde{z})$ is the variable point under integration.

By expressing the $\cos l\tilde{\phi}$ or $\sin l\tilde{\phi}$ in (A 1) in terms of a polynomial of $\cos\tilde{\phi}$, these integrals can be calculated as follows:

$$\left.\begin{aligned} C_0(l, p, A, B, \phi) &= \cos l\phi \; D(l, p, A, B), \\ S_0(l, p, A, B, \phi) &= \sin l\phi \; D(l, P, A, B), \end{aligned}\right\} \tag{A 3}$$

where

$$D(l, p, A, B) = \frac{1}{(A^2+B^2)^{p/2}} \sum_{q=0}^{l} \alpha_{lq} G(q, p, k), \tag{A 4}$$

$$k^2 = \frac{2B^2}{A^2+B^2} = \frac{4\tilde{R}R}{(\tilde{R}+R)^2+z^2} \quad (0 \leqslant k < 1), \tag{A 5}$$

$$\alpha_{00} = 1, \quad \alpha_{lq} = \frac{(-1)^q 2^{2q} l\Gamma(l+q)}{\Gamma(2q+1)\Gamma(l-q+1)}, \tag{A 6}$$

$$G(q, p, k) = \int_0^{\frac{1}{2}\pi} \frac{\cos^{2q}\tau \, d\tau}{[1-k^2\sin^2\tau]^{p/2}}. \tag{A 7}$$

Here $\Gamma(x)$ is the Gamma function. The $G(q, p, k)$ can be related to the complete elliptic integrals $K(k)$ and $E(k)$ of the first and second kinds through the recurrence formulas. These formulas are exact mathematically, but they turn out to be numerically unstable unless k is close to unity, say $k \geqslant 0.90$.

For $k \leqslant 0.90$, we find $B^2/A^2 = k^2/(2-k^2) < 0.681$ and thus can expand the denominator of (A 1) in a series of B^2/A^2 to obtain

$$D(l, p, A, B) = \frac{2\tau}{A^p} \sum_{s=0}^{\infty} \beta_{l+2s, l, p} \, u^{l+2s}, \tag{A 8}$$

where

$$u = \frac{B^2}{A^2} = \frac{2\tilde{R}R}{\tilde{R}^2+R^2+z^2}, \tag{A 9}$$

$$\beta_{00p} = 1, \quad \beta_{l+2s, l, p} = \frac{1}{2^{p+2s}} \frac{(2l+4s+p-2)!!\,\Gamma(l+2s+1)}{(2l+4s)!!\,\Gamma(s+1)\Gamma(l+s+1)}. \tag{A 10}$$

To explain the meaning of k, we can see from (A 5) that k reaches the maximum at $\tilde{R} = (R^2+z^2)^{\frac{1}{2}}$. If $z = 0$ we would have $k = 1$ at $\tilde{R} = R$, a singularity for the integrals in (A 1) or (A 7). The values of $k \geqslant 0.90$ correspond to the interval $((1-k_c)/(1+k_c))\,R \leqslant \tilde{R} \leqslant ((1+k_c)/(1-k_c))\,R$ for the case of $z = 0$, or to a smaller neighbourhood of $\tilde{R} = (R^2+z^2)^{\frac{1}{2}}$ for the case of $z \neq 0$. Here $k_c = (1-(0.90)^2)^{\frac{1}{2}}$. Outside such a neighbourhood we have $k \leqslant 0.90$. If $z \geqslant (2k_c/0.90)\,R$, the whole plane wall $(1 \leqslant \tilde{R} < \infty)$ would correspond to $k \leqslant 0.90$.

In the range of $k \leqslant 0.90$, we are also able to perform the integration over $\tilde{R}$ in (16*c*) analytically by integrating (A 8) term by term with respect to $\tilde{R}$. In the range of $k \geqslant 0.90$, the integration with respect to $\tilde{R}$ can also be performed analytically by expanding the complete elliptic integrals, relating to $G(q, p, k)$ in (A 4), in terms of its complementary modulus $k' = (1-k^2)^{\frac{1}{2}}$, if the collocation point is on the plane wall $(z = 0)$. However, if the collocation point is not located on the plane wall, the

integration over $\tilde{R}$ has to be performed numerically for the part where $k \geqslant 0.90$. If an interval $(b_1\, b_2)$ covers both the ranges of $k \leqslant 0.90$ and $k \geqslant 0.90$, it should be divided accordingly and then appropriate formulas should be used in each of the subintervals. The detailed derivation and formulas can be found in Yan (1985).

Numerical tests show that the algorithms listed herein can reduce the computation time for $H_{ij}^{(\beta)}(R, \phi, z; b_1, b_2; m)$ to a few thousandths of the time required by a numerical quadrature and give an accuracy to at worst 10^{-7} for $m = 0$–7 and $\beta = 1$–3.

REFERENCES

Batchelor, G. K. 1976 *J. Fluid Mech.* **74**, 1.

Brenner, H. 1961 *Chem. Engng Sci.* **16**, 242.

Brenner, H. & Gaydos, L. J. 1977 *J. Colloid Interface Sci.* **58**, 312.

Dagan, Z., Pfeffer, R. & Weinbaum, S. 1982 *J. Fluid Mech.* **122**, 273.

Dagan, Z., Weinbaum, S. & Pfeffer, R. 1982*a* *J. Fluid Mech.* **115**, 505.

Dagan, Z., Weinbaum, S. & Pfeffer, R. 1982*b* *J. Fluid Mech.* **117**, 143.

Dagan, Z., Weinbaum, S. & Pfeffer, R. 1983 *Chem. Engng Sci.* **38**, 4.

Davis, A. M. J. 1983 *Intl J. Multiphase Flow* **9**, 575.

Davis, R. E. & Acrivos, A. 1966 *Chem. Engng Sci.* **21**, 681.

Ganatos, P., Pfeffer, R. & Weinbaum, S. 1978 *J. Fluid Mech.* **84**, 79.

Ganatos, P., Pfeffer, R. & Weinbaum, S. 1980 *J. Fluid Mech.* **99**, 755.

Ganatos, P., Weinbaum, S. & Pfeffer, R. 1982 *J. Fluid Mech.* **124**, 27.

Gluckman, M. J., Pfeffer, R. & Weinbaum, S. 1971 *J. Fluid Mech.* **50**, 705.

Goldman, A. J., Cox, R. G. & Brenner, H. 1967 *Chem Engng Sci.* **22**, 637.

Haberman, W. L. & Sayre, R. M. 1958 *David W. Taylor Model Basin Rep. No.* 1143, Washington D.C.

Happel, J. & Brenner, H. 1973 *Low Reynolds Number Hydrodynamics*, 2nd edn. Noordhoff.

Ladyzhenskaya, O. A. 1963 *The Mathematical Theory of Viscous Incompressible Flow*, Chap. 3, Gordon & Breach.

Leal, L. G. & Lee, S. H. 1982 *Adv. Colloid Interface Sci.* **17**, 61.

Lee, S. H. & Leal, L. G. 1982 *J. Colloid Interface Sci.* **87**, 81.

Leichtberg, S., Pfeffer, R. & Weinbaum, S. 1976 *Intl J. Multiphase Flow* **3**, 147.

Lewellen, P. C. 1982 Hydrodynamic analysis of microporous mass transport, Ph.D. dissertation, University of Wisconsin–Madison.

Miyazaki, T. & Hasimoto, H. 1984 *J. Fluid Mech.* **145**, 201.

Rallinson, J. M. & Acrivos, A. 1978 *J. Fluid Mech.* **89**, 191.

Sadhal, S. S. & Johnson, R. E. 1983 *J. Fluid Mech.* **126**, 237.

Wang, Y., Kao, J., Weinbaum, S. & Pfeffer,R. 1986 On the inertial impaction of small particles at the entrance to a pore including hydrodynamic and molecular wall interaction effects. *Chem. Engng Sci.* (in press).

Weinbaum, S. 1981 Lectures on Mathematics in Life Sciences. *Am. Math. Soc.* **14**, 110.

Yan, Z. 1985 Three-dimensional hydrodynamic and osmotic pore entrance phenomena, Ph.D. dissertation, The City University of New York.

Yan, Z., Shan, H. & Dagan, Z. 1987 The axisymmetric rise of a bubble at the exit of a circular orifice in the presence of insoluble surfactant caps. *Int Conf. on Fluid Mech., The Chinese Soc. of Theo. and Appl. Mech., Beijing, China, June 16–19, 1987.*

Yan, Z., Weinbaum, S. & Pfeffer, R. 1986 On the fine structure of osmosis at the entrance and exit of biological membrane pores, *J. Fluid Mech.* **162**, 415.

Youngren, G. K. & Acrivos, A. 1975 *J. Fluid Mech.* **69**, 377.

Youngren, G. K. & Acrivos, A. 1976 *J. Fluid Mech.* **76**, 433.